Characterization of somatostatin receptor type 2A intracellular trafficking in cells co-expressing somatostatin receptor type 2A and 5

Yingzhou Edward Pan

Department of Neurology and Neurosurgery
Montreal Neurological Institute
McGill University, Montreal
August 2015

Supervisor:
Thomas Stroh, Ph. D.

A thesis submitted to McGill University in partial fulfillment of the requirements of the degree of Master of Science in Neurological Sciences

Acknowledgements

I wish to express my sincere gratitude to my supervisor, Dr. Thomas Stroh for giving me the opportunity to work with him. I arrived with very little experience and understanding of the project on which I was embarking. During the last two years, your guidance has helped me develop my scientific abilities and autonomy. This project would not have been possible without your support.

To Walaa Alshafie, thank you for all your help during this project and for being willing to share your previous experiences. Being able to discuss results as well as ideas for experiments with you has been invaluable and has made this project more than it otherwise would have been.

To Naomi Takeda, thank you for all your help with all administrative matters and help keeping the lab running smoothly. Thank you also for organizing all the out of lab activities. Those have made a huge difference in the last two years.

To Mariette Lavallée, thank you for patiently teaching me cell culture. Thank you also for keeping such excellent records of all things related to lab management. It has made keeping track of the lab after your retirement much easier.

To Steven Silvestrin and all my friends from the Pack and Jones lab, thanks for making the last two years so enjoyable. It wouldn't have been the same without all you.

Contribution of Authors

In Goal 1, the pharmacological experiments with brefeldin A to investigate the intracellular compartment where sst_{2A} is sequestered was done in collaboration with Walaa who designed the experiments. From design to interpretation, the experiments for the characterization of the trafficking pathway of sst_{2A} by co-localization with Rab markers was my work.

In Goal 2, the experiments to gauge the recycling of sst_{2A} using monensin were designed by Walaa Alshafie, a Ph.D. student in our lab. I collaborated with her on data gathering and analysis as well as results interpretation.

The development of the covarianceDetector program for co-localization analysis was my work with help from Matthew Krause, Spencer Fabricant, and James Austin with regards to finding individual functions and operations in MatLab.

This thesis was written entirely by me and was edited by Dr. Stroh and proofread by Naomi Takeda and Walaa Alshafie. The French abstract was edited by Dr. Stroh and Jonathan Côté.

Table of Contents

Abstract

Somatostatin exerts a primarily inhibitory effect across multiple physiological systems, including endocrine and exocrine secretions, through a family of 5 G-protein coupled receptors named somatostatin receptor 1 through 5 (sst_1-sst_5). In AtT-20 cells which primarily co-express sst_2 and sst_5, sst_2 has been shown to remain at the plasma membrane when stimulated for 40 minutes with the sst_2-selective agonist L-779,976 while stimulation with the non-selective agonist [D-Trp^8]-SOM-14 resulted in near complete internalization of sst_{2A}. Unpublished observations showed that following L-779,976 stimulation, sst_{2A} fluorescence at the plasma membrane was lowest after 20 minutes before increasing and plateauing by 40 minutes. We therefore hypothesize that sst_{2A} internalizes then dynamically recycles back to the plasma membrane upon L-779,976 stimulation. Our results showed that sst_{2A} internalizes via Rab5 pathways, recycles via Rab11 pathway, and is not targeted towards Rab9 degradative pathways. Within the cell, sst_{2A} is partially stored in the TGN but the majority is stored in a distinct, syntaxin 6-positive compartment. To help with this investigation, a novel piece of software called covarianceDetector was developed for the targeted detection of co-localization in immunofluorescent images.

Résumé

La somatostatine exerce un effet d'inhibition sur plusieurs systèmes physiologiques, principalement sur la sécrétion des substances endocriniennes et exocrines, par l'intermédiaire d'une famille de 5 récepteurs couplés aux protéines G nommés récepteur de somatostatine 1 à 5 (sst_1-sst_5). Dans les cellules AtT-20 qui expriment surtout le sst_2 et le sst_5, le sst_2 demeure à la membrane cellulaire suivant 40 minutes de stimulation par le L-779,976, un agoniste sélectif pour le sst_2, alors que la même stimulation par l'agoniste non-sélectif [D-Trp^8]-SOM-14 produit une internalisation quasi-complète du sst_2. Des observations non-publiées ont montré que la stimulation avec le L-779,976 produit une expression minimale du sst_2 à la membrane cellulaire après 20 minutes de stimulation avant d'augmenter à un niveau constant après 40 minutes. Nous proposons donc l'hypothèse que le L-779,976 cause une internalisation du sst_2, mais que ce dernier est rapidement recyclé vers la membrane cellulaire. Nos résultats indiquent que le sst_{2A} est internalisé par la voie du Rab5, recyclé par la voie du Rab11 et qu'il n'est pas dégradé par la voie du Rab9. Dans la cellule, il est partiellement stocké dans le réseau trans-golgien mais la plus grande partie est stocké dans un autre compartiment pourvu de syntaxine 6. Afin de rendre la détection de colocalisation de protéines plus rapide et facile, un nouveau logiciel nommé covarianceDetector (détecteur de co-variabilité) a été développé.

Chapter One: Introduction

1. Introduction

1.1 Somatostatin

Somatostatin is a peptide hormone whose primary function is the inhibition of endocrine and exocrine secretions (Cuevas-Ramos and Fleseriu 2014). A 14 amino acid long version was first isolated from sheep hypothalamic extract by Brazeau et al. (1973). The second version of somatostatin was isolated later from pig intestines (Pradayrol et al. 1978) and found to be 28 amino acids long, elongated at the N-terminus (Pradayrol et al. 1980). Both somatostatin 14 (SOM-14) and somatostatin 28 (SOM-28) are generated from a 116 amino acid long prepro-SOM that is then cleaved into a 92 amino acid long pro-SOM before being further processed into either form of the peptide (Cuevas-Ramos and Fleseriu 2014).

Functionally, the active region of both SOM-14 and SOM-28 is located primarily from amino acid 7 to amino acid 10. Exploratory experiments with single amino acid mutations of this region produced analogs with much lower potency for growth hormone inhibition compared to endogenous somatostatin (Janecka, Zubrzycka, and Janecki 2001). As such, this region, which in endogenous somatostatin forms a β-loop, has been the primary site of study in the synthesis of peptide somatostatin analogs (Patel 1999). The first agonist to have a higher potency than the endogenous somatostatin was a minimally modified SOM-14 called [D-Trp^{8}]-SOM-14, in which the 8th amino acid was switched from a L-conformation tryptophan to a D-conformation tryptophan (Rivier, Brown, and Vale 1975). This single modification made [D-Trp^{8}]-SOM-14 eight times more potent than native SOM-14. It also had the benefit of making [D-Trp^{8}]-SOM-14 much more metabolically stable, giving it a half-life in the hundreds of minutes vs. the 3 minutes

of native SOM-14. It is a modification that would be incorporated into the design many other synthetic SOM peptide agonists such as octreotide (Janecka, Zubrzycka, and Janecki 2001).

1.2 Somatostatin Effect and Distribution

While most well-known to act within the central nervous system, somatostatin exerts an inhibitory effect in multiple physiological systems and is accordingly expressed in several cellular populations.

Within the CNS, somatostatin is known primarily as an inhibitor of endocrine secretion. Somatostatin produced in neurons of the hypothalamus, more specifically of the paraventricular nucleus, arcuate nucleus and ventromedial nuclei (Johansson, Hökfelt, and Elde 1984), reaches the anterior pituitary where it inhibits the secretion of growth hormone (Brazeau et al. 1973), prolactin, thyroid stimulating hormone (Vale et al. 1974) and adrenocorticotropic hormone (ACTH) (Richardson and Schonbrunn 1981). Additionally, somatostatin has also been found in many other regions of the CNS, particularly in the cortex but also across several nuclei such as the caudate, putamen, hippocampus and spinal trigeminal nucleus to name but a few (Finley et al. 1981) though somatostatin seems to be absent from the cerebellum (Johansson, Hökfelt, and Elde 1984). This widespread distribution of somatostatin and its ability to act as a neuromodulator (Epelbaum 1986) could underlie the links between somatostatin and many neurological pathologies, which are discussed in more detail in the next section.

Outside the nervous system, somatostatin continues to exhibit a primarily inhibitory effect in the organs where it is expressed. In the gastrointestinal tract (GIT), somatostatin is primarily expressed in neurons of the myenteric plexus (Patel 1999) and inhibits the production of many gastric hormones including cholecystokinin, gastric inhibitory peptide, gastrin and secretin as well as exocrine secretions such as peptisongen and hydrochloric acid (Møller et al.

2003). In the pancreas, somatostatin is expressed by cells within the islets but distinct from the glucagon and insulin secreting cells that it inhibits (Dubois 1975; Boden et al. 1986; Alberti et al. 1973). Somatostatin's inhibition of endocrine secretion has been exploited as a treatment for hormone secreting adenomas. In patients with acromegaly, growth hormone levels returned in normal in 53% of patients given the clinical somatostatin agonist octreotide (Ezzat et al. 1992).

Additionally, somatostatin possesses anti-proliferative effects. In cultured cells, somatostatin stops HeLa cell proliferation induced by epidermal growth factor by inhibiting the separation of centrosomes (Mascardo and Sherline 1982). In vivo, somatostatin's anti-proliferative characteristics have been shown in various pituitary adenomas. In growth hormone secreting tumours, treatment with somatostatin clinical agonists octreotide and lanreotide can control tumour growth in 97% of patients (Bevan 2005) and reduce tumour size in 50% of patients (Melmed 2006).

1.3 Clinical Relevance of Somatostatin and Somatostatin Receptors

Somatostatin and its receptors' many physiological functions have linked it with several diseases and in some cases, led to a form of treatment. For example, its inhibitory effect on endocrine secretion have made somatostatin agonists a staple of pituitary tumour treatments (Heaney and Melmed 2004). Its neuro-modulatory inhibitory effects have suggested that somatostatin may play a role in temporal epilepsy (Robbins et al. 1991; Buckmaster et al. 2002). Finally, correlative studies have also suggested that somatostatin may play a role in neurodegenerative diseases such as Alzheimer's disease and Parkinson's disease (Epelbaum 1986).

Clinically, somatostatin receptors are primarily targeted in the context of pituitary adenomas. Pituitary adenomas cause problems through two mechanism: the dysregulated

secretion of hormones into systemic secretion and the compression of surrounding brain structures as they grow (Heaney and Melmed 2004). Today, the use of synthetic somatostatin agonists is the most common non-surgical method of treating pituitary adenomas. For example, patients suffering from acromegaly are typically treated with the synthetic somatostatin agonists octreotide and lanreotide. However, while this treatment works very well in 45% to 65% of patients (Ben-Shlomo and Melmed 2008; Heaney and Melmed 2004), it nevertheless leaves between a third to half of the patients unresponsive to treatment. The most likely explanation for patients who are unresponsive is an internalization of the somatostatin receptors (Hofland and Lamberts 2003). A better understanding of the trafficking mechanism of somatostatin receptors and the properties of agonists that cause their internalization could lead to the treatment of more effective pharmacological treatments.

Somatostatin-based treatments are currently limited to the treatment of adenomas, but other neurological have also been linked to somatostatin and show promise in the development of somatostatin-based treatments. For example, temporal epilepsy has been linked to a decreased somatostatin expression in the dentate gyrus, likely from the loss of somatostatin-producing interneurons, and an increase in somatostatin receptors, possibly as a compensatory mechanism (Robbins et al. 1991). A later study in somatostatin knock out mice suggested that somatostatin acts as a mild anticonvulsant. Compared to wild type mice, somatostatin knock out mice were more sensitive to seizures with shorter latency between kainic acid administration, more intense seizure phenotypes and a higher mortality rate (Buckmaster et al. 2002). This suggests that somatostatin may play a causal role in epilepsy as a “protective” mechanism, making it a promising therapeutic target for temporal lateral epilepsy treatment (Binaschi, Bregola, and Simonato 2003). Another example is the link between somatostatin and neurodegenerative

diseases. Although here, a causal link has yet to be established, somatostatin expression has been shown to increase in the striatum of Huntington's chorea, but decrease in the cortex of demented Parkinson's disease and Alzheimer's disease (Epelbaum 1986). In one study by Craft et al. (1999) showed that administration of 150mg/h of somatostatin in patients with Alzheimer's disease increased their performance in declarative memory tasks, a promising result for the development of treatments.

1.4 Somatostatin Receptors

Somatostatin's ability to inhibit proliferation and hormone secretion is mediated through a family of 5 receptors labeled somatostatin receptor 1 through 5, with somatostatin receptor 2 (sst_2) expressed in two alternative splicing forms labeled sst_{2A} and the C-terminus shorter sst_{2B} (Cuevas-Ramos and Fleseriu 2014). Cloning the genes for the receptors during the 1990s allowed the elucidation of their structures. The structure of somatostatin receptors alternates between hydrophilic and hydrophobic regions; it was later confirmed that somatostatin receptors were part of the 7-transmembrane domain G-Protein Coupled Receptor (GPCR) superfamily (Patel 1999).

Not all receptors subtypes are expressed at every somatostatin target site. Instead, each receptor has distinctive expression sites, which in turn, gives each target site a distinct combination of somatostatin receptors. For example, within the brain, the cortex expresses high levels of sst_1 and sst_2, the hippocampus expresses a low amount of all receptors while the hypothalamus almost exclusively expresses sst_5. In other organs, there seems to be a correlation between hormone secreting organs and sst_2 expression. Non-endocrine organs like the heart and spleen express sst_4 and sst_3 respectively, with very low to no expression of sst_{2A} respectively. By contrast, the adrenal glands express high levels sst_2; the islet cells of the pancreas express high

levels sst_{2A} and low levels of sst_4; and the anterior pituitary primarily expresses sst_2 and sst_5. Reviewed by Patel et al. (1995).

While the subpopulation of somatostatin receptors expressed does not change in between the normal pituitary and pituitary adenomas, the expression levels may vary depending on the type of adenoma. In growth hormone secreting adenomas, sst_2 and sst_5 remain the dominant receptors expressed (Reubi et al. 2001). However, in ACTH secreting adenomas, while sst_2 and sst_5 remain the most expressed receptors, sst_2 expression is lower than in WT pituitary due to the over-secretion of cortical hormones (Cuevas-Ramos and Fleseriu 2014). In cultures, the ACTH-secreting pituitary adenoma mouse cell line AtT-20 overexpresses both sst_{2A} and sst_5 (Ben-Shlomo et al. 2009).

Structurally, the somatostatin receptors all follow the same basic layout of G-protein coupled receptors with seven hydrophobic transmembrane domains. The third intracellular loop and the C-terminus tail contain phosphorylation sites for receptor internalization (Jacobs and Schulz 2008). Of note is that all somatostatin receptors also contain a putative PDZ domain binding site that could serve for the interaction of somatostatin receptors with scaffolding proteins (Kreienkamp 2002).

1.5 Somatostatin Agonist

The endogenous SOM-14 is non-selective, binding strongly to all 5 somatostatin receptors with an IC_{50} of 1.1nM to 2.1nM. SOM-28, on the other hand, is selective for sst_5, binding with an IC_{50} of 0.25nM for sst_5, but an IC_{50} from 2.8nM to 5.4nM for the other receptors. (Patel et al. 1994).

Given the wide range of hormones somatostatin can inhibit and the distinctive subpopulation of somatostatin receptors expressed at each target site, synthetic somatostatin agonists have been actively developed towards the goal of clinical treatments, particularly for hormone secreting adenomas. Because endogenous somatostatin has a very short half-life of 1-3 minutes (Janecka, Zubrzycka, and Janecki 2001) and is non-selective (Patel et al. 1994), development of synthetic agonists have focused on both increasing the metabolic stability, receptor subtype specificity and potency of analogs.

One of the earliest analogs produced was [D-Trp^{8}]-SOM-14 by Rivier, Brown & Vale in 1975. This agonist is identical to endogenous SOM-14 but with the tryptophan in the 8th position replaced with a D-conformation tryptophan. This simple substitution made [D-Trp^{8}]-SOM-14 eight times more potent than its endogenous counterpart (Rivier, Brown, and Vale 1975). Furthermore, it also increased the functional half-life of [D-Trp^{8}]-SOM-14 and all future peptide incorporating this modification by two orders of magnitude, up to hundreds of minutes, by preventing enzymatic degradation (Janecka, Zubrzycka, and Janecki 2001). The modification, however, did not confer receptor subtype specificity to [D-Trp^{8}]-SOM-14 (Janecka, Zubrzycka, and Janecki 2001), so work continued towards selective agonists.

Work towards identifying the protein domain in SOM-14 that was responsible for its inhibitory activity eventually identified the region between the 6th and 11th amino acids as being particularly important and lead to the development of SMS 201-995, today better known as octreotide (Janecka, Zubrzycka, and Janecki 2001). Synthesized in the 1980s, octreotide is a short octapeptide whose central four amino acids mimic the 7th to 10th amino acids of [D-Trp^{8}]-SOM-14, including the [D-Trp] modification (Bauer et al. 1982). It was first considered "selective" in the sense that it was 45 times more effective at inhibiting growth hormone

secretion than SOM-14, but only twice as potent as SOM-14 at inhibiting insulin secretion (Bauer et al. 1982). That octreotide was in fact selective for sst_{2A} and sst_5 would be discovered later (Lamberts et al. 1996). Finally, because octreotide is stable, with a half-life of around two hours (Janecka, Zubrzycka, and Janecki 2001), it is now widely used for somatostatin analog therapies (Patel 1999).

But octreotide remains a peptide analog and in general, these tend to have short elimination half-lives and, importantly for a clinical treatment, poor oral bioavailability which is why non-peptide analogs have also been pursued (Janecka, Zubrzycka, and Janecki 2001). L-779,976 is one such agonist. L-779,976 was randomly assembled as part of the Merck chemical collection among 200 000 other putative agents. Functional studies that measured the dose of L-779,976 required to inhibit forskolin-induced production of cAMP showed that it is a very potent somatostatin agonist, with an IC_{50} of 0.1nM. Furthermore, L-779,976 is highly selective for sst_2. In competition binding assays performed on isolated CHO cell membranes, L-779,976 had a Ki of 0.05nM for sst_2 compared to at least 310nM for sst_4 or 4260nM for sst_5, a 6 000 or 80 000 fold preference for sst_2 respectively (Rohrer et al. 1998). Although L-779,976 never made it to the clinic, its high potency and selectivity has resulted in its use in basic research requiring a selective sst_2 agonist (Strowski et al. 2000; Emery et al. 2002; Sharif et al. 2007).

1.6 Somatostatin Receptor Downstream Signalling

As G-protein coupled receptors, somatostatin receptor activation can lead to modulation of multiple second-messenger systems with multiple downstream consequences. Three key ones are the inhibition of the adenylyl cyclase-cAMP-PKA pathway, the regulation of intracellular

calcium concentration and modulation of the phosphoprotein phosphatase pathways (Ben-Shlomo and Melmed 2010; Csaba and Dournaud 2001).

One of the best studied pathways downstream of somatostatin receptors is the adenylyl cyclase – cyclic AMP – protein kinase A signalling pathway. Upon stimulation by an agonist, all five somatostatin receptors activate their inhibitory G-protein, leading to the inhibition of adenylyl-cyclase and a subsequent decrease in cAMP concentration (Patel et al. 1994). This decrease occurs relatively quickly: *in vivo* studies conducted in the anterior pituitary showed a significant decrease in cAMP within two minutes of somatostatin application (Borgeat et al. 1974). Functionally, inhibition of this pathway has been primarily linked with somatostatin's ability to inhibit endocrine secretions. In cultured AtT-20 cells, somatostatin was capable of negating ACTH release induced by forskolin upregulating cAMP levels (Heisler et al. 1982). In conceptually similar experiments done *in vivo,* somatostatin completely blocked growth hormone secretion induced by growth hormone-releasing factor, though cAMP was only partially reduced (Bilezikjian and Vale 1983), suggesting that other mechanisms are also involved in the inhibition of endocrine secretion.

Somatostatin receptors also inhibit hormonal secretion through modulation of intracellular calcium concentration (Ben-Shlomo and Melmed 2010). In vivo studies in rat showed that somatostatin stimulation directly inhibited calcium channels (Shapiro and Hille 1993). But somatostatin also regulates intracellular Ca^{2+} concentration through indirect mechanisms. In AtT-20 pituitary cell cultures as well as in primary neuron cultures, activation of the Gαi subunit of the receptor-associated G-protein inhibits inward rectifying K^+ channels (Takano et al. 1997). This inhibition of K^+ currents causes the plasma membrane to hyperpolarize. As the membrane hyperpolarizes, spontaneous action potential firing rate

decreases, the intracellular concentration of calcium also decreases, leading to inhibition of hormone exocytosis (Tsaneva-Atanasova et al. 2007; Patel 1999).

The anti-proliferative effects of somatostatin, however, seem to be mediated through phosphoprotein phosphatase pathways. SHP-1 is a phosphotyrosine phosphatase activated upon stimulation of sst_2 (Florio 2008). It mediates its anti-proliferative effects by inducing cell cycle arrest at the G1 phase (Pagès et al. 1999). Another pathway inhibited by phosphotyrosine phosphatases is the MAPK pathway. MAPK pathway activation is known to play an important role in cell proliferation (Seger and Krebs 1995) and somatostatin receptor activation has caused phosphotyrosine phosphatase-mediated inhibition of MAPK itself as well as other members of the pathway such as Raf1 in several cell lines (Ben-Shlomo and Melmed 2010; Csaba and Dournaud 2001), suggesting an important anti-proliferative function for somatostatin signaling.

1.7 Somatostatin Receptor Trafficking

Being GPCRs, somatostatin receptors are subject to the same desensitization and trafficking mechanisms that underlie the regulation of most GPCRs. For all their diversity, the majority of GPCRs will internalize with a relatively predictable pattern. Stimulation leads to the phosphorylation of the 3rd intracellular loop of GPCRs by G-protein coupled receptor kinases (GRKs) (Pitcher, Freedman, and Lefkowitz 1998). This phosphorylation event allows for the recruitment of other proteins such as β-arrestins, which ensure the decoupling of GPCRs from their G-proteins, mediating desensitization of the receptor (Benovic et al. 1987). Internalization is then induced by the binding of recruiting proteins like adaptor protein 2 (AP-2) which recruit and assemble the clathrin which serves to the formation of clathrin-coated pits through which GPCRs internalize (Laporte et al. 1999).

Once internalized, GPCRs can be categorized in two broad categories based on their trafficking patterns, which interestingly, correlate with their binding affinity and stability with β-arrestins. Class A GPCRs, like the β2-adernergic receptor, favour β-arrestin2 over β-arrestin1 but only bind transiently, losing their interaction with β-arrestin2 once internalized. These receptors tend to be recycled very quickly back to the plasma membrane following internalization (Oakley et al. 2000; Anborgh et al. 2000; Seachrist and Ferguson 2003). By contrast, Class B GPCRs, like the angiotensin II type 1A receptor, do not exhibit a preference for β-arrestin 1 or 2, but will bind very stably to either β-arrestin, remaining in a complex even after endocytosis. These receptors are usually either degraded or sequestered for a long time before being recycled (Anborgh et al. 2000; Oakley et al. 2000; Seachrist and Ferguson 2003). It should be noted that this is a general rule and that not all GPCRs adhere to this pattern (Seachrist and Ferguson 2003).

Under resting conditions, sst_2 is primarily localized to the plasma membrane (Sarret et al. 2004) and upon stimulation, is internalized into the trans-Golgi network (Csaba et al. 2007). In studies performed in HEK293 cells, Tulipano et al. (2004) demonstrated that stimulated sst_{2A} binds in a stable manner with β-arrestin, suggesting that it should be a class B GPCR. While several studies suggest that sst_2 is eventually recycled to the plasma membrane rather than being degraded (Jacobs and Schulz 2008), the timing of that recycling is less certain. In Tulipano's HEK293 cells, sst_2 recycled quickly back to the plasma membrane within 40 minutes (Tulipano et al. 2004). However, *in vivo* studies performed in the rat hippocampus showed that while stimulated sst_2 internalized from dendrites to the TGN in a matter of minutes, it required up to 48 hours before re-establishing a control-like distribution (Csaba et al. 2007). Considering the models used, the physiological in-vivo study bears more weight, suggesting that sst_2 behaves as a

class B GPCR. Indeed, in our own observations in AtT-20 cells, which endogenously express sst_2 and sst_5, internalized sst_2 takes up to 24 hours to recycle to the plasma membrane at levels comparable to unstimulated cells.

By contrast, somatostatin receptor 5 behaves like a typical class A GPCR. It forms a very transient interaction with β-arrestin (Tulipano et al. 2004) and is very quickly recycled back to the plasma membrane upon stimulation (Stroh et al. 2000). Sst_5's resting localization, however, bears a special mention. Unlike sst_{2A}, sst_5 is primarily localized within the TGN of the cell under resting conditions. Upon stimulation, the population present at the cell surface internalizes but induces a fast recruitment of the intracellular pool of receptors, establishing a dynamic equilibrium that ensures a constant presence of active receptors at the cell surface (Stroh et al. 2000).

Of particular interest to the study of somatostatin receptor trafficking is the ability of the different receptor subtypes to affect each other's trafficking as demonstrated in a study performed by Sharif et al in 2007. When sst_2 was stably transfected into Chinese hamster ovary cells (CHO_{sst2}), stimulation with the non-selective agonist [D-Trp^8]-SOM-14 and the sst_2-selective agonist L-779,976 both resulted in very efficient internalization of sst_2. However, in CHO cells stably transfected with both sst_{2A} and sst_5 (CHO_{sst2+5}), as well as in AtT-20 pituitary adenoma cells which endogenously express both receptors, stimulation with L-779,976 caused sst_{2A} to remain localized at the plasma membrane. Yet stimulation with [D-Trp^8]-SOM-14 caused sst_{2A} to internalize like it did in CHO_{sst2} cells. The interpretation at the time was that the presence of *unstimulated* sst_5 seemed to have inhibited the internalization of stimulated sst_{2A}. However, this interpretation has since changed and in this thesis, I demonstrate that following

stimulation with L-779,976 in cells expressing both sst_{2A} and sst_5, sst_{2A} does internalize but quickly recycles back to the plasma membrane.

The mechanism underlying the observation was not elucidated at the time. Though there have been studies that suggest that heterodimerization of somatostatin receptors could modulate their trafficking (Grant et al. 2008; Grant and Kumar 2010), in the case of the 2007 study, fluorescent images taken of the cell showed very clear segregation of sst_{2A} and sst_5 at all times (Sharif et al. 2007), indicating that another mechanism is likely at work. One possibility is that of a TGN resident sorting protein differentially regulating the two.

1.8 Investigation of the trans-Golgi apparatus with markers and pharmacological agents

The trans-Golgi Network is a major trafficking hub in the cell, sorting not only cargo from the ER and cis Golgi to its correct target but also managing vesicles coming from the endocytic pathway (Gu, Crump, and Thomas 2001). It would therefore be very useful to have reliable markers for this subcellular compartment. In the aforementioned sst_2 internalization studies done in hippocampus, sst_2's intracellular localization in the trans-Golgi network compartment was determined based on co-localization with two different trans-Golgi network markers: Syntaxin 6 and TGN38 (Csaba et al. 2007). A third option is PIST, a PDZ domain sorting protein that is also primarily localized to the TGN (Wente et al. 2005).

TGN38, was first identified and cloned by Luzio et al. (1990) and was found to be exclusively located to the trans-Golgi network. TGN38 maintains its TGN localization through a cytoplasmic tyrosine-containing domain (Bos, Wraight, and Stanley 1993). While it was later found that TGN does move to the plasma membrane before being internalized again, the vast

majority of TGN38 in the cell at steady state remains in the TGN, making TGN38 an excellent marker for that compartment (Roquemore and Banting 1998).

Syntaxin 6 is another protein localized to the TGN (Bock et al. 1997) and has been used as a marker in co-localization studies (Sarret et al. 2004; Csaba et al. 2007). Syntaxin6 is part of the SNARE family of proteins, which are involved in the final steps of vesicle trafficking, namely, vesicle docking and fusion. SNARE's can be categorized based on their compartmental location: v-SNAREs on vesicles and t-SNAREs on target membranes. SNAREs mediate vesicle fusion through the formation of a *trans*-SNARE complex; as vesicles approach their target membrane, v-SNARES will bind to cognate t-SNAREs and a SNARE-motif present in both groups of SNAREs will mediate the formation of a very stable helical core complex. This brings the membrane of the vesicles in close enough proximity to the target membrane to mediate membrane fusion (Jahn and Scheller 2006; Hong 2005; Fasshauer 2003).

Syntaxin 6 is a t-SNARE first identified by Bock, Lin and Scheller as being a TGN resident protein whose function was the docking of vesicles with the TGN (Bock, Lin, and Scheller 1996; Bock et al. 1997; Jahn and Scheller 2006). Additionally, Syntaxin 6 has been implicated in different function within other compartments (Jung et al. 2012). Outside the TGN, Syntaxin 6 has been localized on early endosomes and found to interact directly with the Rab5 effector EEA1 (Simonsen et al. 1999), suggesting that Syntaxin 6 could play a role in early endosomal trafficking. In endothelial cells, Syntaxin 6 is present in early endosomes and inhibition of its function causes α5β1 integrin molecules to be misrouted towards a late endosomal degradative pathway rather than a recycling pathway (Tiwari et al. 2011). In endocrine cells, the homotypic fusion of secretory granules which underlies their maturation is dependent on a Syntaxin 6-Syntaxin 6 homotypic interaction (Wendler et al. 2001). Thus,

proteins co-localized with Syntaxin 6 outside the TGN could reasonably be dependent on the function of Syntaxin 6 for appropriate trafficking within the cell.

Another TGN marker of particular interest in the study of somatostatin receptors is PIST. When colabeled with TGN38, PIST was found to overlap perfectly with the TGN marker, indicating that it was localized exclusively to the TGN (Chen et al. 2012). PIST was first described in 2001 (Neudauer, Joberty, and Macara) as a PDZ-domain protein interacting specifically with Tc-10, hence its name. More than a TGN marker, PIST has been shown to interact directly with sst_5 and mediates the TGN localization of sst_5 through the PDZ-domain interaction (Wente et al. 2005). While it is not known if sst_2 interacts with PIST, sst_2 internalizes to the TGN (Csaba et al. 2007) and also possess a PDZ-domain binding site (Kreienkamp 2002), making a putative interaction a reasonable expectation.

In addition to using marker proteins, the TGN can also be studied using pharmacological agents. Brefeldin A and monensin are two particularly useful ones.

Brefeldin A is used in protein trafficking investigation by inhibiting protein trafficking within the endomembrane system. Its best known effect is the reversible disassembly of the trans-Golgi network in animal cells (Wagner et al. 1994; Sciaky et al. 1997). Brefeldin A's mode of action is through the inhibition of Arf1, a small GTPase that mediates the recruitment coat proteins required for vesicle formation at the Golgi apparatus (Jackson and Casanova 2000). At first, this seems to create a paradox: Sciaky et al. reported a movement of cis-Golgi enzymes back into the endoplasmic reticulum, which seemingly shouldn't be possible without vesicles budding off the cis-Golgi cisterna. Nebenführ, Ritzenthaler and Robinson (2002) propose that in fact, this inability for vesicles to bud off the Golgi apparatus is precisely what causes the

apparent retrograde transport. Unable to bud off, the vesicles expressing v-SNARE eventually bind with cognate t-SNAREs located on the endoplasmic reticulum and will end up dragging their entire cis-Golgi cisterna towards the ER and causes a membrane fusion event. Meanwhile, as Brefeldin A does not prevent cisternae maturation, the trans-Golgi cisternae and TGN continue to mature and eventually are lost to the cytoplasm.

Monensin is a pharmacological agents used to investigate protein trafficking by inhibiting exocytosis. Monensin's mode of action is tied to its chemical nature. As an ionophore, monensin breaks down proton gradients by shuttling back and forth across membranes, exchanging protons for Na^+, particularly at the Golgi apparatus. This exchange causes not only a loss of acidification, but also an increase in osmolar pressure, leading to a characteristic swelling of the Golgi apparatus in cells treated with monensin. However, in spite of this morphological change, monensin causes minimal side effects and is able to inhibit the exocytosis of cargo from the Golgi apparatus without altering protein synthesis, at even low concentrations (0.01 - 1μM). Monensin acts primarily at the Golgi apparatus and it is sufficiently well established that its ability to block the exocytosis of a protein is typically interpreted as a sign that that protein's trafficking pathway involves the Golgi apparatus. Reviewed by Mollenhauer, Morré and Rowe (1990).

1.9 Rab Proteins act as vesicular markers

Rab proteins are small GTPases that serve to coordinate the trafficking activity in eukaryotic cells. Rabs can be activated into their GTP-bound, "on" state by guanine nucleotide exchange factors (GEFs). Following activation, Rabs have intrinsic GTP to GDP hydrolysis properties that will deactivate them in time, but this process is greatly accelerated by GTPase-activating proteins (GAPs) (Delprato, Merithew, and Lambright 2004). Inactive, GDP-bound

Rabs are stabilized by Rab GDP dissociation inhibitors (GDI) that also act to increase the cytosolic solubility of the inactive Rabs (Ullrich et al. 1993). The ability of Rabs to coordinate trafficking events is not due to intrinsic properties of the Rabs themselves, but to their ability to recruit a very wide variety of effector proteins that bind to active, GTP-bound Rabs. The variety of these effectors is the reason Rabs are involved in almost every step of trafficking and can serve a very diverse set of function such as sequestering cargo, recruiting endocytotic proteins, tethering vesicles to motor proteins for trafficking and targeting of cargo towards a specific site. Because Rabs are key regulators of membrane trafficking between intracellular organelles, they can be used as a marker for endosomal identity, allowing the distinction, for example of early endosomes from recycling endosomes (Stenmark 2009).

Rab5 GTPase is a marker for the endocytic pathway, present at the plasma membrane, on endocytic vesicles, and in sorting endosomes (Woodman 2000) where it coordinates several functions (Zerial and McBride 2001). Before endocytosis even begins, Rab5 promotes the sequestration of cargo proteins, such as the transferrin receptor, into the site of endocytosis (Bucci et al. 1992). Rab5 then promotes the recruitment of clathrin to form the clathrin coated pits (McLauchlan et al. 1998). Rab5 also seems to play a role in the motility of early endosomes as functional inhibition of Rab5s significantly decreases the tethering of early endosomes to microtubules (Nielsen et al. 1999).

Going in the other direction, Rab11 is a marker for the recycling trafficking pathway. Functionally, Rab11 has been shown to be key to the recycling of transferrin receptors (Ullrich et al. 1996). Functionally, Rab11 mediates late recycling by tethering recycling endosomes stemming from the Golgi apparatus to the actin-attached motor protein myosin Vb (Roland et al. 2007). Myosin Vb is a motor protein that travels towards the cell periphery along actin filaments

and that has been shown to mediate the transport of AMPA receptors towards dendritic spines (Wang et al. 2008).

Rab9 is a marker for late endosomes and degradative pathway and is key to the formation of lysosomes. Newly synthesized lysosomal enzymes in the TGN need to be shuttled by mannose 6-phosphate receptors (M6PR) into late endosomes where they are released. The function of Rab9 in late endosomes is to rescue M6PR from degradation by trafficking it back to the TGN before late endosomes mature into lysosomes. Failure to do so, induced by a dominant negative form of Rab9, resulted in a decrease in M6PR recycling and an associated decrease in ability to target lysosomal hydrolase towards the lysosomes (Riederer et al. 1994). Rab9 accomplishes its function through an effector protein, TIP47 (Díaz and Pfeffer 1998). TIP47 is a cytosolic protein that acts as an adaptor protein that binds to the cytoplasmic domain of M6PR and the GTP-bound active form of Rab9 (Díaz and Pfeffer 1998). A particularly interesting observation is that binding to Rab9 actually increases the affinity of TIP47 for M6PR, which serves to increase the efficiency of M6PR late endosome to TGN trafficking (Carroll et al. 2001).

1.10 Transferrin trafficking

Transferrin is the iron transporting protein of the blood. In its iron bond form, it binds to transferrin receptors at the surface of the cell and is internalized with it. Within the endosomes, acidification to a pH of 5.5 causes transferrin to change its conformation and to release the iron it was transporting. Transferrin, however, remains bound to its receptor until both have travelled back through the recycling pathway arrive to the plasma membrane, at which point it is released back into the bloodstream (Gkouvatsos, Papanikolaou, and Pantopoulos 2012).

Studies have shown that the transferrin receptor internalizes via Rab5 positive, clathrin coated vesicles (Bucci et al. 1992) and recycle via Rab11 positive vesicles (Ullrich et al. 1996).

The fact that the transferrin ligand remains bound throughout the process makes it a powerful investigative tool. Trischler, Stoorvogel and Ullrich (1999) used biotinylated-transferrin to investigate the biochemical compositions of the various endosomes along the transferrin pathway, using tagged transferrin to label the endosomes. Likewise, it can be reasonably expected that fluorescently labeled transferrins would be able to fluorescently tag both Rab5 and Rab11 positive vesicles and could be used to validate an immunocytochemistry protocol targeted against Rab5 or Rab11.

1.11 Co-localization analysis in multichannel images

The markers of intracellular compartments and vesicles explored in the previous sections are critical to immunocytochemistry, where proteins of interest and compartment markers are labeled with various fluorophores using specific antibodies. By determining whether or not the two fluorophores co-localize within the cells, it becomes possible to know whether a protein travels through a specific compartment as it is trafficked within the cell. Accurate co-localization analysis is therefore equally crucial for accurate trafficking pathway characterization. In their review paper, Dunn, Kamocka and McDonald (2011) describe the main methods of co-localization analysis and quantification and consider some of their strengths and pitfalls.

Visual interpretation is the most intuitive and widely used method of co-localization analysis. The investigator overlays both images in their respective colours and looks for intermediate shades in the composite image. For example, yellow would be the intermediate shade between a red channel and a green one. The benefits of this method are its ease and intuitiveness. The problem, however, is that intermediate shades between the two channels' colours only appear if they are of comparable brightness. If one channel is systematically brighter than the other, intermediate shades may not appear visually at all.

Another visualization method is the scatterplot. In scatterplot, each pixel in the image is plotted in the graph based on its brightness in one channel along the x-axis and its brightness in the other channel along the y-axis. Co-localization in a scatterplot is determined based on the distribution of the points. The scatterplot of two very well co-localized proteins will typically have the resulting point cloud shaped as a line along the graph. The benefit of a scatterplot is its ability to reveal co-localization even when one channel is systematically brighter than the other as this will simply shift the point cloud closer to one axis. Scatterplots can also reveal the difference between two populations of co-localized pixels if a different channel dominates in both populations. For example, if one channel is brighter in one cell, but the second channel is brighter in a second cell, a scatterplot can reveal two separate point clouds. The problem with scatterplot is that it remains a non-quantitative method. Furthermore, the aligned point cloud remains an ideal-case condition. In reality, the point-cloud may be quite diffuse and the scatterplot itself does not set a threshold for the "tightness" of the point cloud along a line required for co-localization.

To quantify co-localization, the most commonly used method is the Pearson's Correlation Coefficient (PCC), calculated as:

$$PCC = \frac{\sum_i (R_i - \bar{R}) * (G_i - \bar{G})}{\sqrt{\sum_i (R_i - \bar{R})^2 * \sum_i (G_i - \bar{G})^2}}$$

where R_i and G_i are the brightness intensities in pixel i within the red and green channels respectively, and $\bar{R}$ and $\bar{G}$ are average intensity across the entire channels. The PCC value ranges from 1 for two perfectly identical channels to -1 where the brightness values across the channels are perfectly inversed. The strength of the PCC is that, because it subtracts the mean brightness value from each individual pixel value, it is capable of giving a correlation score even if one

channel is far brighter than the other and boils pixel variability to one number. The PCC method, however, is not without its caveats too. PCCs calculated based on whole images can be artificially high due to the inclusion of black pixels representing non-biological regions such as the coverslip. Alternatively, PCCs can be made artificially low if two distinct populations have different dominant channels, as explored in the discussion on scatterplots. To diminish these artifacts, PCCs are best calculated based on selected regions of interests (ROIs) that both exclude black, non-biological pixels, but also segregate distinct populations. Even with ideal ROIs, PCCs remain a mostly internal comparison tool. With the exception of very high PCCs near 1, intermediate values between 0 and 1 have the same problem as scatterplots: there is no clear threshold for co-localization. Instead, PCCs are more commonly used to compare different treatment conditions to gauge a relative increase or decrease in co-localization. Reviewed by Dunn, Kamocka and McDonald (2011).

A plugin for ImageJ is available that implements the calculation of a PCC for any two images. Simply called “Co-localization Finder” (Bourdoncle 2006), it takes as input a pair of grayscale images representing the two channels to be analyzed and computes the PCC for the two images. It generates a data table with the PCC along with a scatter plot of the images. It goes one step further by generating a composite image of the two original grayscale images false-coloured in red and green, and highlights the pixels that are plotted in different sections of the scatterplot. This allows, in theory, to determine which regions in the original images are co-localized.

1.12 Hypothesis and Aims

1.12.1 Hypothesis

A study performed in our lab by Sharif et al. (2007) has shown an effect of sst_5 on the trafficking of sst_2. In CHO_{sst2+5} and AtT-20 cells, 40 minutes of selective stimulation of sst_2 by L-779,976 caused sst_2 to remain at the plasma membrane rather than internalizing. Interestingly, this phenotype was not seen in CHO_{sst2} cells stimulated with L-779,976 nor in any of the three cell line if the non-selective somatostatin agonist [D-Trp^8]-SOM-14 was used. In these conditions, sst_2 internalized as expected of a stimulated GPCR. The interpretation at the time was that the presence of unstimulated sst_5 somehow inhibited the internalization of sst_2.

That interpretation changed recently as a result of a serendipitous observation. In AtT-20 cells, stimulation by L-779,976 was ended at finer time points between control and 40 minutes. We observed a decrease in surface expression of sst_2, reaching a minimum at 20 minutes before reappearing at the plasma membrane by 40 minutes.

I therefore hypothesized that selectively stimulated somatostatin receptor 2 is internalized and recycled to the plasma membrane in the presence of unstimulated somatostatin receptor 5. My primary goal was to characterize the full trafficking pathway of sst_2 by colabeling it with markers of intracellular trafficking such as Rab5, Rab9, Rab11 as well as markers of the TGN like PIST and Syntaxin 6. The secondary goal was a confirmatory study of sst_{2A} recycling by inhibiting exocytosis using monensin.

1.12.2 Primary Goal: Characterizing the Trafficking Pathway of sst_2

Previous studies have investigated the ability of various agonists to induce somatostatin receptors signalling and internalization in various systems (Jacobs and Schulz 2008; Patel 1999)

but no studies have investigated the actual pathway of somatostatin receptor 2. To investigate the trafficking pathway of sst_2, I colabeled it with various markers of intracellular trafficking.

Because GPCRs in general are known to internalize via clathrin-coated vesicles (Laporte et al. 1999), I colabeled sst_2 with Rab5 for the internalization pathway. Sst_2 was colabeled with Rab11 for the recycling pathway since Rab11 acts on recycling endosomes budding from the Golgi apparatus, the target site of monensin activity. Rab9 was used as the marker for late endosomal degradative pathway. To confirm that sst_2 internalizes into the TGN, sst_2 was colabeled with the TGN markers PIST as well as Syntaxin 6 following stimulation. Cells were also incubated with Brefeldin A and stained with sst_2 and TGN markers to observe whether or not its intracellular pool is disrupted along with the TGN.

1.12.3 Secondary Goal: Pharmacological Investigation of sst_2 Recycling

The drug monensin is known for its ability to inhibit exocytosis of vesicles in cells (Mollenhauer, James Morré, and Rowe 1990). In this part of my project, I incubated AtT-20 cells in monensin for 10 minutes then stimulated them, still in the presence of monensin, with [D-Trp^8]-SOM-14 or L-779,976 before fixing and staining them for sst_{2A} using immunocytochemistry. The sst_{2A} localization patterns of these cells were compared to cells treated equivalently, but without monensin to further determine whether or not our hypothesis that sst_{2A} internalizes and recycles is correct.

Chapter Two: Materials and Methods

2.1 Cell Culture

AtT-20 cells were cultured in 25cm^2 vented, culture flasks (Corning #: 430639) with DMEM culture medium (Gibco#: 12100-061) with 3.7g/L of $NaHCO_3$, 10%$_{v/v}$ foetal bovine serum (FBS) (Gibco#: 10082-147), and 1%$_{v/v}$ Penicillin/Streptomycin (Gibco#: 15140-122). A serum-free version of DMEM was also made for fluorescent-transferrin experiments. Cells were kept in an incubator set to 37°C with 5% atmospheric CO_2 and a tray of water for humidity.

Cells were split 3 times a week on Mondays, Wednesdays and Fridays when they reached approximately 90% confluence. Prior to splitting cells, all mediums were warmed to 37°C in a hot-water bath for at least 40 minutes. Culture medium in the flasks was poured out and the cells were rinsed twice with 5mL TTBS (3.025g/L tris base, 8g/L NaCl, 0.373g/mL $MgCl_2 \bullet 6H_2O$, 0.338g/L KCl, 0.1g/L Na_2HPO_4, and 0.057g/L $CaCl_2$). Cells were then detached from the flask floor by incubating them in 2mL of 0.05% trypsin-EDTA (Gibco#: 25300-062) for 5 minutes. Flasks were knocked gently to detach cells if necessary. 3mL of culture medium was added to rinse the flask and the total volume was transferred to a 15mL centrifuge tube (Corning#: 430790) and centrifuged for 5 minutes at 1000 rpm. The supernatant was poured away and the pellet was resuspended in 10mL of DMEM. For flasks scheduled to be split in two days (Mon-Wed, Wed-Fri), 3.5mL of resuspended cell solution and 8.5mL DMEM were combined into one flask. For flasks to be split in 3 days (over weekend) or in 4 days (Mon-Fri), 2.0mL and 1.5mL resuspended cell solution were added respectively and filled to 12mL in the flask.

2.2 Cell Stimulation

Cells destined for experiments were taken from the resuspended cell solution and seeded on poly-L-lysinated #1.5 coverslips (Fisher#: 12-545-81) in 4-well plates (Nuncleon#: 176740). 150 000 cells were seeded within 1mL of DMEM per well and left to grow overnight. If the experiment required labeling cells with Alexa647-labeled transferrin, cells were cultured in pre-warmed, serum-free DMEM for two hours prior to stimulation. At the time of the experiment, cells were removed from the incubator and the DMEM was replaced by 1mL of pre-warmed Earle's (+) (1L ddH2O, 8.18g NaCl, 0.376g KCl, 0.264g CaCl2, 0.183g MgCl2●6H2O, 5.95g Hepes, pH balanced to 7.4, 0.1%$_{m/v}$ bovine serum albumin, 0.09%$_{m/v}$ glucose) for 10-40 minutes. Cells were maintained at 37°C by placing the 4 well plates in a hot water bath platform that immersed only the bottom 3mm of the plates in 37°C water. If the experiment required incubation with monensin or brefeldin A, then 25µM of monensin or 10µM of brefeldin A was added to the Earle's (+) and to all subsequent stimulation solutions.

Stimulation was initiated by aspirating the Earle's (+) and adding Earle's (+) with either 100nM [D-Trp^{8}]-SOM-14 or 100nM L-779,976, along with 1:5000 Transferin$_{Alexa647}$ and/or pharmacological agents if the experiment called for it. Stimulation was ended by aspiration of the stimulation solution and addition of 1mL per well of 4°C Earle's (+) and placing the 4 well plates on an ice bed.

2.3 Fixing, Immunofluorescent labeling, Mounting and Imaging

Cells were rinsed twice 500µL 0.1M PBS (1L ddH_2O, 1.794g NaH_2PO_4●H_2O, 12.35g Na_2HPO_4) before being fixed by incubation in 4%$_{w/v}$ paraformaldehyde in 0.1M PBS for 20 minutes. Cells were then rinsed twice in 500µL 0.1M PBS, then twice more with 0.1M TBS (1L ddH_2O, 12.1g trizma base (Sigma, Ref#: T1503), 9g NaCl, pH adjusted to 7.4 using HCl). Cells were then incubated in 500µL blocking buffer (0.1M TBS, 0.05%w/v Saponin, 5%v/v NGS,

2%w/v BSA) for 15 minutes. Cells were then labeled in 300µL of primary antibody solution (0.1M TBS, 0.05%w/v Saponin, 0.5%v/v NGS, primary antibodies) before the 4 well plates were sealed with parafilm (Parafilm#: #PM992) and incubated overnight at 4°C. The next day, cells were rinsed twice with 500µL 0.1M TBS before being incubated in 500µL of fluorescent secondary antibodies (diluted in 0.1M TBS) for 40 minutes. Cells were rinsed two more times in 0.1M TBS.

Coverslips were removed from their wells by tweezers and dipped in ddH_2O, blotted dry, and mounted, cell-side-down, onto a microscope slide with poly-aquamount. The slides were left to dry for a minimum of 3 hours before imaging.

Imaging was performed on a Zeiss LSM 710 confocal microscope with a 63x 1.4NA oil-immersion objective. Coverslips belonging to the same experiment were imaged at a 1024x1024 pixel resolution with equivalent settings. Digital gain and digital offset were left at 1 and 0 respectively and pinhole was set to 1 airy unit. Images were optimized using laser power and sensor gain.

2.4 Data analysis

This project relies primarily on the detection of co-localization between two, sometimes three fluorophores. To this end, the primary analysis method was visually targeted profile analyses.

Within the ZEN image analysis program, lines were drawn across regions visually deemed to be likely sites of co-localization. A region was deemed to be the site of co-localization if the brightness along the drawn line exhibited aligned peaks. This process, however, was time consuming, inefficient and prone to false negatives if one channel vastly outshines the other.

Cell surface brightness analyses were also performed to measure the presence of sst_{2A} at the plasma membrane. In the ZEN software, a tracing tool was used to define the plasma membrane around individual cells. The brightness profile was exported from ZEN into Microsoft Excel and the average along individual traces was calculated. Brightness was normalized to the no stimulation, no monensin condition as control. Statistical significance was determined using a 1-factor ANOVA and Tukey's post hoc comparison test with a $P < 0.05$.

2.5 Automated covarianceDetector

In order to accelerate the co-localization detection process, a custom piece of MatLab software was developed simply called *covarianceDetector*. Unlike previously existing imageJ plugins like "colocalizationFinder...," which determine co-localization based on Pearson's Co-localization Coefficient (PCC) and highlights pixels in a composite image based regions of the scatterplot, *covarianceDetector* works on entirely different principles.

In a manual fluorescence intensity profile analysis where a line is drawn across a region of the multichannel image, brightness is graphed on the Y-axis and physical space along a line is plotted along the X-axis. A segment of the X-axis is considered to be the site of co-localization if the trace for both channels within that segment increase together, peak around the same point along X and then decrease together.

covarianceDetector replicates this manual profile analysis procedure, which is the reason it is called "covariance" detector rather than "co-localization" detector. Rather than defining points of co-localization based on PCC, *covarianceDetector* takes a very geometric approach to detecting co-localization. A digital image can be visualized as a grid laid flat on a horizontal surface, with each cell within the grid "painted" a different shade of grey ranging from black to white based on the number stored in each square (0 for black, 255 for white in an 8-bit image).

However, if instead the numbers are made to represent the height of a column, then a topographical hillside literally rises out of what used to be an image, the elevation at any one cell correlated with the brightness at that point, creating "hills." With hills comes the ability to measure the "steepness" of those hills at every point along their surface. At every point, one could stick a flagpole, making sure it is perpendicular to the ground at that specific point. The steeper the hill, the smaller the angle between the flagpole and a true horizontal plane will be. If two plots of land of equal size are gridded out and paired flagpoles are planted at corresponding points across the two fields, then it is possible to determine how similar the two fields are at every single pair of points by comparing the orientation of each flagpole pair. This is exactly what *covarianceDetector* does.

covarianceDetector is composed of a series of "modules," each of which accomplishes part of the task to compare the two "hill-containing fields" that it analyzes in the form of a pair of grayscale images. The titular module called *covarianceDetector* is the coordinator that handles the files and ensures that pairs of images are fed to the subsequent modules.

The first module is a low-pass filter called *averagerSlaved* that simply removes noise from both images. The methodology employed is a typical low-pass filter one: the number contained within a particular cell is replaced by the average of its value and of the cells around it, usually in a grid of 3x3 with the pixel being averaged at the centre. This removes high-frequency noises and allows the program to detect the trends present without being thrown off by individual bright, noise pixels.

After both images have been filtered for noise, they are fed through *topographerSlaved*. *topographerSlaved* is the "flagpole planter" of the program. At each point in each image, it

computes a normal vector of length 1. Because any vector in 3D space can be broken down into its fundamental components in the X, Y and Z axis, *topographerSlaved* creates 3 new matrices and sorts into each one the X, Y or Z component of the normal vector at that particular point. *topographerSlaved* thus overall outputs two sets of 3 matrices, each set representing one of the two images, the three matrices storing the X, Y and Z components of every normal vector.

These 6 matrices are fed to *comparatorSlaved* where the actual comparison of each normal vector is performed by performing a dot-product on each pair of normal vectors. Because each normal vector has a set length of 1, the possible range of values is from -1 to 1. Parallel normal vectors will give a dot-product of 1, anti-parallel normal vectors give a dot-product of -1 while perpendicular normal vectors will give a dot-product of 0. *comparatorSlaved* generates a new, single matrix, the covariance matrix, with each cell containing the dot-product of each pair of normal vectors at that particular coordinate. This is the critical step that determines if the two channels "co-vary" or "anti-vary" at any particular coordinate.

Before a final image is generated, an "importance" score needs to be given to each value within the covariance matrix by the *cosWeighterSlaved* module. This is done to solve a problem generated by black regions in images. Black regions are topographically equivalent, with normal vectors pointing almost straight up in the Z-axis direction. They are thus given covariance scores of near 1 by *comparatorSlaved*. But these regions where brightness is constant are of no interest to an investigator; high-interest regions are those where the brightness is changing in both channels.

To ensure pixels in low-interest regions are discarded without resorting to setting arbitrary brightness threshold values, *cosWeighterSlaved* considers the angle between each

normal vector and the horizontal XY-plate. Indeed, regions where brightness is changing quickly will have normal vectors that form very small angles relative to the XY-plane while regions where brightness is constant have normal vectors that form a near 90° angle with the XY-plane, as is the case in black pixels. For the two channels in each pixel, *cosWeighterSlaved* calculates the average angle that the two normal vectors make relative to the XY-plane and takes the cosine of that angle. Flat regions, where the average angle between the two normal vectors and the XY-plane is 90, will thus receive a "cos weight score" of zero, which acts as our "importance score." By contrast, the normal vectors of regions with quickly changing brightness values will have smaller angles relative to the XY plane, and so, higher cosine weights. For every coordinate, *cosWeighterSlaved* multiplies the dot-product of the two normal vectors (how similar the two regions are) by the cosine weight associated with that same region and outputs a final matrix, the weighted covariance matrix.

The choice was made to apply a cosine function to the average angle rather than a linear weight relationship between angle and weight simply because the angles between the normal vectors and the XY plane are not expected to approach values extremely close to zero. Since the cosine function has a small plateau at values near zero, the net effect of using a cosine of the angle is to bias higher weight scores towards expected angles (~10° to 90°) and away from angles smaller than 10° which are not expected to occur.

The final step is to produce an image usable by the investigator. The weighted covariance matrix is fed to *heatmapperSlaved* which generates a colour-coded heatmap illustrating regions with covariance. Regions where the channels are moving in the same direction (increasing or decreasing together) have positive weighted covariance scores that are painted in shades of red. By contrast, regions where the channels are moving in opposite directions will be painted in

shades of blue. Finally, regions where the normal vectors are perpendicular, or far more commonly, where they both point straight up and are thus of no interest and receive a weighted covariance score of zero, are painted in green, which sits at the middle of the visible spectrum.

See supplementary figure 1 for a schematic representation of data flow through *covarianceDetector*.

covarianceDetector wasn't designed as a statistical tool. Rather, it was a designed to facilitate the discovery of co-localization. It should be noted that *covarianceDetector* remains a very prototypical piece of software. Not fully validated nor tested, *covarianceDetector* was not exclusively entrusted with any biological conclusions in the course of this project. Rather, it was used strictly as a targeting solution. Regions painted in red were then investigated through manual profile analysis to determine whether or not those were sites of co-localization. Because it has a slight propensity for false positives, it became particularly useful to confirm the *absence* of co-localization in the sst2 and Rab9 colabeling experiments. It was also used to find more subtle points of co-localization. Its main advantage is its ability to recognize covariance, even if one channel is far brighter than the other. This gives it a very high degree of sensitivity, allowing it to recognize sites of co-localization that other software plugins like "colocalization Finder" may miss. A more thorough discussion of the advantages and pitfalls of *covarianceDetector* is present in the discussion section.

Table 2.1

1° Antibody / Protein	1° Dilution	2° Antibody	2° Dilution
Rb α-sst2A (AbCam: ab134152) (Clone: UMB1)	1:3000	Alexa 488 Gt α-Rb (Molecular Probes: A-11008)	1:500
Ms α-Rab5 (AbCam: ab66746)	1:1000	Cy3 Gt α-Ms (Jackson Immuno: 115-165-146)	1:800
Rt α-Rab11 (AbCam: ab95375)	1:800	Cy3 Dk α-Rt (Jackson Immuno: 712-154-150)	1:800
Ms α-Rab9 (AbCam: ab2810)	1:500	Cy3 Gt α-Ms (Jackson Immuno: 115-165-146)	1:800
Gp α-PIST (Dr. Kreienkamp)	1:10 000	Cy3 Gt α-Gp (Jackson Immuno: 106-165-003)	1:800
Ms α-Syntaxin 6 (Bd Transduction Labs: 610635)	1:5000	Cy3 Gt α-Ms (Jackson Immuno: 115-165-146)	1:800
Transferrin-Alexa647 (Molecular Probes: T23366)	1:1000		

Table 2.1: List of primary antibodies, secondary antibodies and fluorescently tagged proteins used. Primary antibodies diluted in an antibody dilution buffer (0.1M TBS, 0.05%w/v Saponin, 0.5%v/v NGS, primary antibodies) while secondary antibodies were diluted in 0.1M TBS. Guinea pig anti-PIST was generous supplied by Dr. Hans-Jürgen Kreienkamp, University of Hamburg, Germany.

Chapter 3: Results

3.1 Primary Goal: Characterization of the sst_2 trafficking pathway

3.1.1 sst_{2A} co-localizes with Rab5 and Transferrin upon stimulation

To investigate the endocytosis pathway of sst_{2A}, cells were stimulated with L-779,976 and [D-Trp^8]-SOM-14 for 1, 2, 4, 6 and 10 minutes (N=3). They were then labeled for sst_{2A} and Rab5 using immunocytochemistry. Labeling for transferrin trafficking was achieved by using purchased transferrin covalently conjugated to the Alexa-647 fluorophore.

Sst_{2A} began to internalize within a minute of stimulation with either [D-Trp^8]-SOM-14 (Fig 3.1A to E) or L-779,976 (Fig 3.1F to J). Just one minute following stimulation with [D-Trp^8]-SOM-14, vesicles that were fluorescently labeled for sst_{2A}, Rab5 and transferrin became apparent (Fig 3.1A) and were detectable after up to 10 minutes of stimulation (Fig 3.1E). L-779,976 stimulation yielded similar results though sst_{2A} positive vesicle density was a bit lower than in [D-Trp^8]-SOM-14 stimulation during the first two minutes (Fig 3.1F & G).

3.1.3 sst_{2A} co-localizes with Rab11 and Transferrin during L-779,976 stimulation

In order to determine the recycling pathway of sst_{2A} during L-779,976 stimulation, AtT-20 cells were stimulated with L-779,976 for 40 minutes and then labeled for sst_{2A} and Rab11 using immunocytochemistry and for transferrin receptors using the same Alexa647-tagged transferrin used in the Rab5 colabeling experiments (N=3). Sst2A was consistently co-localized with both Rab11 and transferrin within vesicles throughout the cytoplasm of the cells (Fig 3.2).

3.1.4 Sst_{2A} very rarely co-localizes with Rab9 following [D-Trp^8]-SOM-14 or L-779,976 stimulation

GPCRs can be degraded following internalization. In order to determine whether or not sst_{2A} was targeted towards the lysosomal degradative pathway following internalization, AtT-20 cells were stimulated with [D-Trp^8]-SOM-14 and L-779,976 for 20 or 40 minutes and stained for sst_{2A} and the late lysosome marker Rab9 (N=4).

Rab9 exhibited punctate labeling throughout the cytoplasm but remained segregated from sst_{2A} labeling. In the unstimulated conditions, Rab9 labeling was occasionally found to overlap with sst_{2A} present at the plasma membrane (Fig 3.3A&D). However, in these regions, rises in Rab9 signal were not associated with a local rise in sst_{2A} signal (Fig 3.3D&G, Profile 1) or were even associated with a local decrease in sst2A signal (Fig 3.3D&H, Profile 2). In the stimulated conditions, Rab9 vesicles found within the perinuclear pool of sst_{2A} were also often associated with a local decrease in sst_{2A} signal (Fig 3.3C&I, Profile 3) while Rab9 vesicles found in the cytoplasm were simply devoid of sst_{2A} (Fig 3.3C&J, Profile 4).

When the sst_{2A} and Rab9 images were analyzed covarianceDetector, the software reported a general absence of covariance. Red signals along the periphery were not due to co-localization but due to both channels increasing to biological background levels at the limit between the cell and the coverslip. On very rare instances, covarianceDetector reported cytoplasmic covariance that was indeed due to co-localization (Fig 3.3K, arrow). Manual profile analysis (Fig 3.3C&L, Profile 5) confirmed that, although very dim, these regions were the site of true co-localization and not an artifact. However, such co-localization events were very rare and occurred at the same rate across all conditions.

3.1.5 Sst_{2A} partially co-localizes with PIST in the perinuclear region

In order to identify the intracellular compartment where sst_{2A} is sequestered following internalization, AtT-20 cells were stimulated with [D-Trp^8]-SOM-14 or L-779,976 for 40 minutes and stained for sst_{2A} and the TGN marker PIST. The experiment was also repeated in cells incubated with brefeldin A in order to investigate the fate of sst_{2A} if it cannot be sequestered into the TGN (N=4).

Without stimulation, sst_{2A} was localized primarily at the plasma membrane as expected while PIST was localized primarily to a perinuclear region (Fig 3.4A). After 40 minutes of stimulation with [D-Trp^8]-SOM-14, sst_{2A} was primarily located within the perinuclear region. Although sst_{2A} and PIST were then located in the general region of the cell, (Fig 3.4D) a profile analysis reveals that in fact, sst_{2A} and PIST only partially co-localize (Fig 3.4E). While certain sst_{2A} and PIST peaks were aligned, very often, a peak in one signal aligned with a trough in the other. When both channels were analyzed by covarianceDetector, the perinuclear region was revealed to be painted with a great deal of dark blue (Fig 3.4F), indicating that very often, the two channels moved steeply in opposite directions to each other, confirming the observations made in profile analysis. Stimulation with L-779,976 yielded similar results, with sst_{2A} and PIST partially co-localized in the perinuclear region of the cell (Fig 3.4G-I).

Surprisingly, when the experiment was repeated in the presence brefeldin A to disrupt the trans-Golgi network, stimulation with both [D-Trp^8]-SOM-14 and L-779,976 revealed that while the perinuclear build-up of PIST was completely disrupted, sst_{2A} continued to internalize and sequester in what appears to be the same perinuclear region (Fig 3.4J&K, M&N). This was very unexpected and suggested that in addition to the TGN, sst_{2A} was also sequestered in another, brefeldin A-insensitive compartment.

3.1.6 Giantin, PIST and TGN38 are disrupted by brefeldin A, but Syntaxin 6 is not

To ensure that brefeldin A was as effective at disrupting the TGN as the PIST experiments would suggest, cells were incubated for 40 minutes in brefeldin A and stained for 3 different TGN markers: PIST, TGN38 and syntaxin 6, as well as for a cis-Golgi cisterna marker: giantin. Because this was a pilot experiment, it was performed only once.

Across all cells observed, PIST and TGN nuclear localization was very efficiently dispersed in the cytoplasm (Fig 3.5E&F) by brefeldin A compared to control (Fig 3.5A&B). Giantin perinuclear build-up too was greatly reduced by brefeldin A incubation (Fig 3.5D&H). Surprisingly, syntaxin 6 was unaffected by the presence of brefeldin A, maintaining a strong perinuclear presence indistinguishable from control (Fig 3.5D&H).

In cells free of brefeldin A, co-localization experiments showed that syntaxin 6, like sst_{2A}, partially co-localized with PIST (data not shown).

3.1.7 Sst_{2A} co-localizes strongly with syntaxin 6 in the perinuclear region and outside it

In order to determine whether or not sst_{2A} and syntaxin 6 were both located within the same brefeldin A insensitive compartment, AtT-20 cells were stimulated with [D-Trp^8]-SOM-14 or L-779,976 for 40 minutes, with or without brefeldin A and were then stained for sst_{2A} and syntaxin 6 (N=4).

Following stimulation with either agonist, with or without brefeldin A, internalized sst_{2A} showed excellent co-localization with syntaxin 6 (Fig 3.6D,G,J&M). A profile analysis crossing the perinuclear region showed very well aligned peaks of sst_{2A} and syntaxin 6 with little if any anti-variance (Fig 3.6E,H,K&N). When analyzed using covarianceDetector (Fig 3.6F,I,L&O), the perinuclear region was mostly red with very little dark blue, indicating that sst_{2A} and syntaxin 6 co-varied very tightly within that region.

Performing a co-localization analysis with covarianceDetector also revealed that sst_{2A} and syntaxin 6 co-localized quite commonly outside the perinuclear region: at the plasma membrane and within the cytoplasm. The white arrow in Fig 3.6F shows a region of a cell stimulated with [D-Trp^8]-SOM-14 without brefeldin A that covarianceDetector reported as a co-localization site. While the corresponding plasma membrane patch was almost imperceptibly dim (Fig 3.6D, arrow), profile analysis across that region shows that sst_{2A} and syntaxin 6 do indeed co-localize at the plasma membrane (Fig 3.6E, arrow). The arrow in figure 3.6O shows a cytoplasmic zone flagged by covarianceDetector that turned out to be a dim (Fig 3.6M, arrow), but clear co-localization site (Fig 3.6N, arrow) in a cell stimulated with L-779,976 with brefeldin A.

3.2 Secondary Goal: Pharmacological Confirmation of sst_2 Recycling

3.2.1 Monensin abolishes surface sst_2 fluorescence in L-779,976 stimulated AtT-20 cells

AtT-20 cells were pre-incubated in 10μM of monensin or not, and then stimulated with the sst_{2A} selective agonist L-779,976 or the non-selective [D-Trp^8]-SOM-14 or left unstimulated in the presence or absence of monensin.

In unstimulated, monensin-free cells, sst_{2A} fluorescence was primarily located at the plasma membrane (Fig 3.7A). In unstimulated cells incubated with monensin, sst_{2A} distribution remained identical, being primarily located at the plasma membrane (Fig 3.7B). In cells stimulated for 40 minutes with the non-selective agonist [D-Trp^8]-SOM-14, sst_2 almost completely internalized into a perinuclear pool, leaving very little sst_2 at the plasma membrane, regardless of the presence or absence of monensin (Fig 3.7C&D).

However, monensin did have an effect on cells stimulated with L-779,976. In cells stimulated with L-779,976 for 40 minutes without monensin, sst_{2A} was present both in the

perinuclear pool and at the plasma membrane (Fig 3.7E). By contrast, in cells incubated in monensin and stimulated with L-779,976, sst_{2A} was present exclusively within the perinuclear region and absent from the plasma membrane (Fig 3.7F), making these cells indistinguishable from [D-Trp^8]-SOM-14 stimulated cells.

Peripheral brightness analysis showed that L-779,976 with monensin was statistically significantly dimmer than L-779,976 alone ($p<0.05$), at ~25% of control as opposed to ~50% (Fig 3.8).

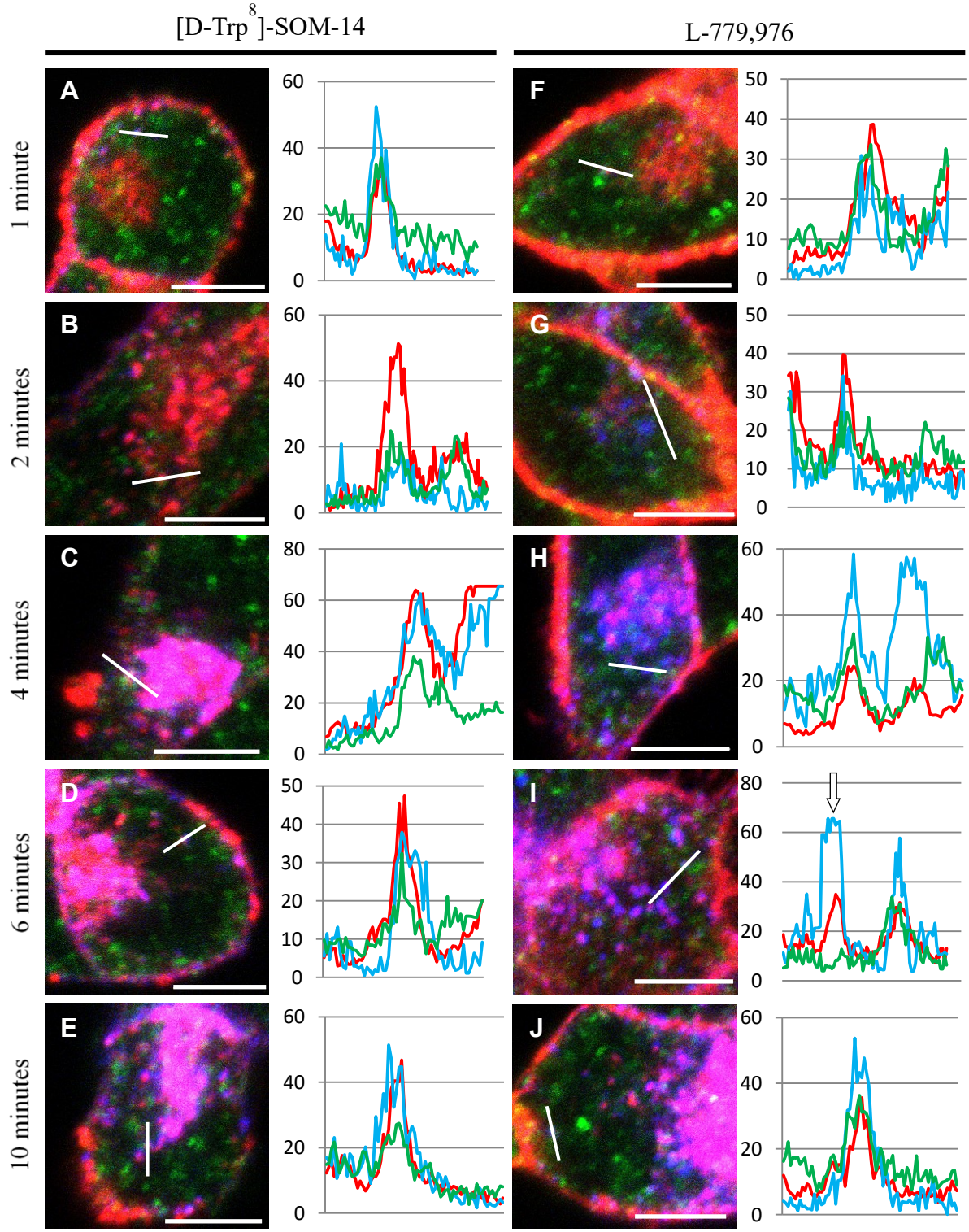

Fig 3.1: AtT-20 cells stimulated with [D-Trp8]-SOM-14 or L-779,976 stained for sst2A, Rab5 and Transferrin: Upon stimulation with either [D-Trp^8]-SOM-14 (A-E) or L-779,976 (F-J), sst_{2A} can be seen in vesicles that are also stained for Rab5 and transferrin. Brightness profile analyses performed on these vesicles (white bar & graph on right) show that at all time points and with either agonist, brightness peaks for sst_{2A}, Rab5 and transferrin line up very precisely. This suggests that sst_{2A} internalizes via Rab5 positive, clathrin coated vesicles. In the L-779,976 condition, some vesicles contained a peak for sst_{2A} and transferrin, but not Rab5, suggesting that these vesicles are recycling back towards the plasma membrane (I, arrow). Images were captured with very high gain in order to reveal the vesicular fluorescence, which saturated plasma membrane fluorescence (A,F&G) and perinuclear pool fluorescence where sst_{2A} and transferrin are seen to build-up (C-E,I,J). N=3

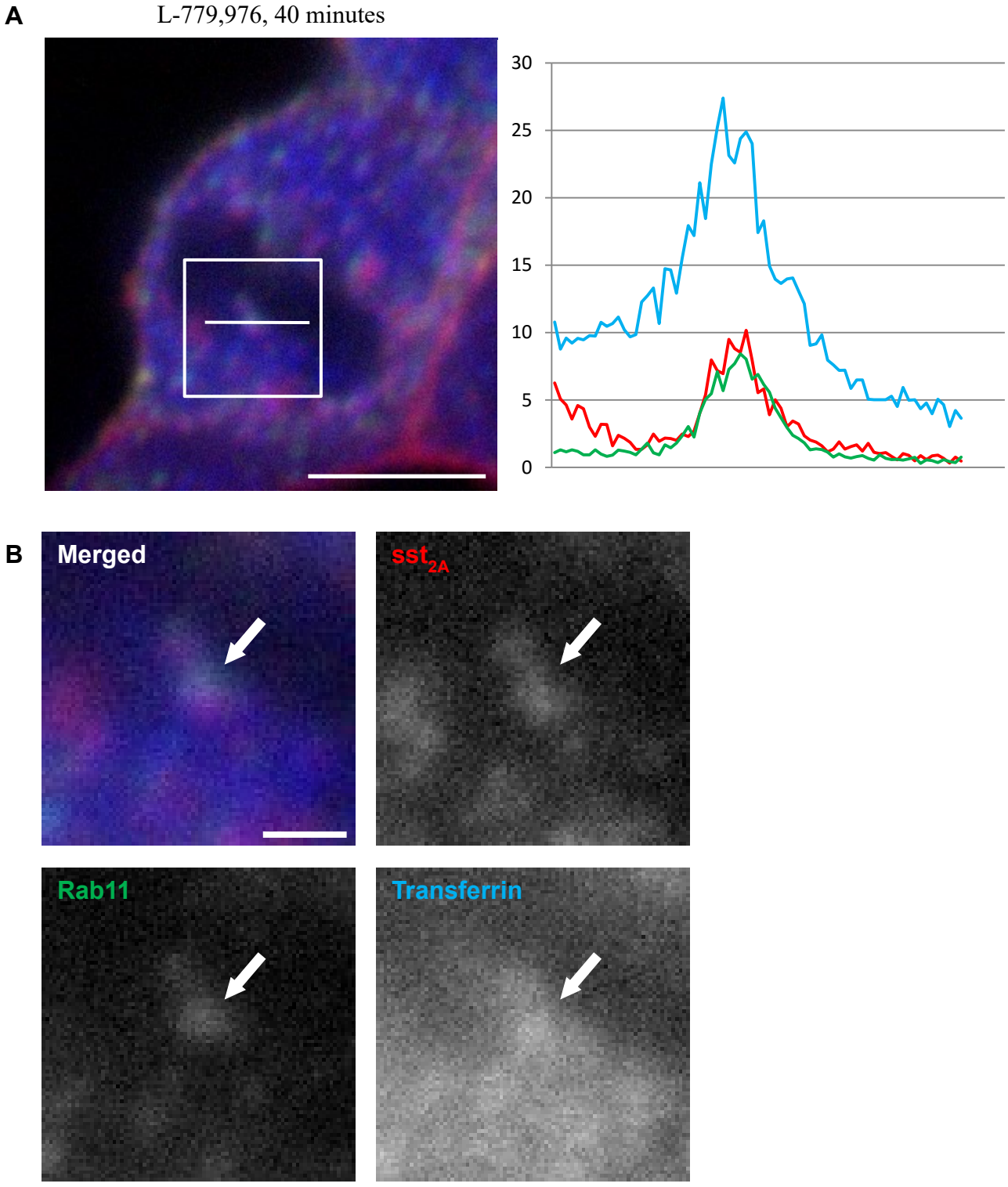

Fig 3.2: AtT-20 cells stimulated with L-779,976 for 40 min, immunostained for sst2A, Rab11 and Transferrin: After 40 minutes of L-779,976 stimulation, sst_{2A} can be seen in vesicles that are also positive for Rab11 and transferrin (A, left). A profile analysis (A, white line & graph on right) shows that the fluorescence peaks for sst_{2A}, Rab11 and transferrin line up very well, suggesting that all three proteins are present within a specific vesicles. Panel B shows an enlarged view of the box in Panel A and the individual channels in that region. White arrows point out a specific vesicle stained for all three proteins. This suggests that sst_{2A} recycles via Rab11 positive vesicles with L-779,976 stimulation. Scalebar A=5µm, B=2µm. Gamma = 0.45 N=3

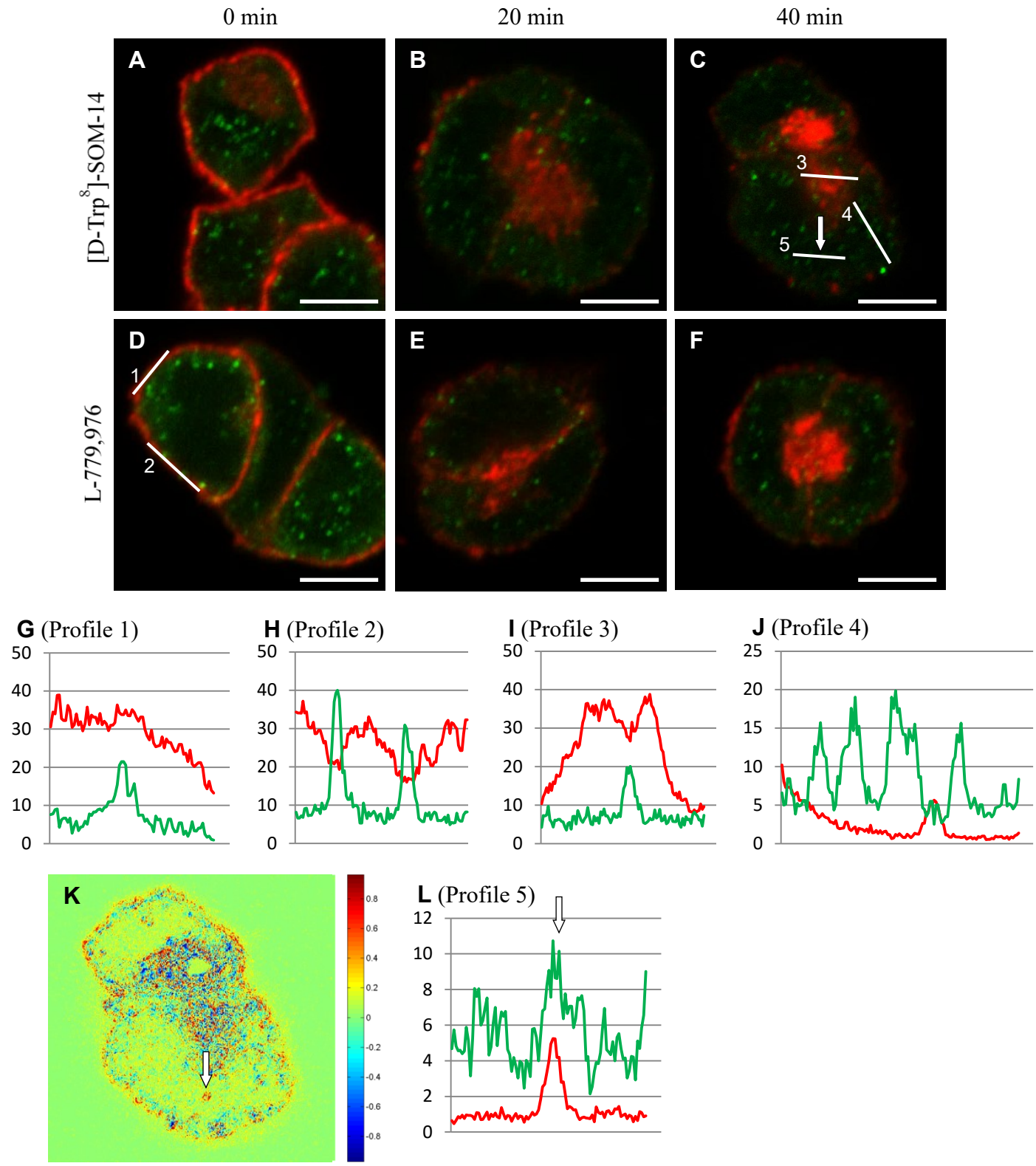

Fig 3.3: AtT-20 cells stimulated with L-779,976 or [D-Trp8]-SOM-14 for 20 minutes or 40 minutes and immunostained for sst2A and Rab9: Across all conditions, sst_{2A} and Rab9 remain well segregated (A-F). Rab9 at the plasma membrane is either not associated with an increase in sst_{2A} signal (G) or associated with a local decrease in sst_{2A} immunoreactivity (H). Rab9 in the perinuclear region of stimulated cells is also often associated with a local decrease in sst_{2A} signal intensity (I) while Rab9 in the cytoplasm is not associated with any sst_{2A} immunofluorescence (J). CovarianceDetector can detect very rare instances of sst_{2A} and Rab9 co-localization (solid arrow K, L) at the same occurrence rate across all conditions, suggesting that while sst_{2A} degrades in small amounts, it is not actively targeted towards lysosomal degradation following stimulation. N=4

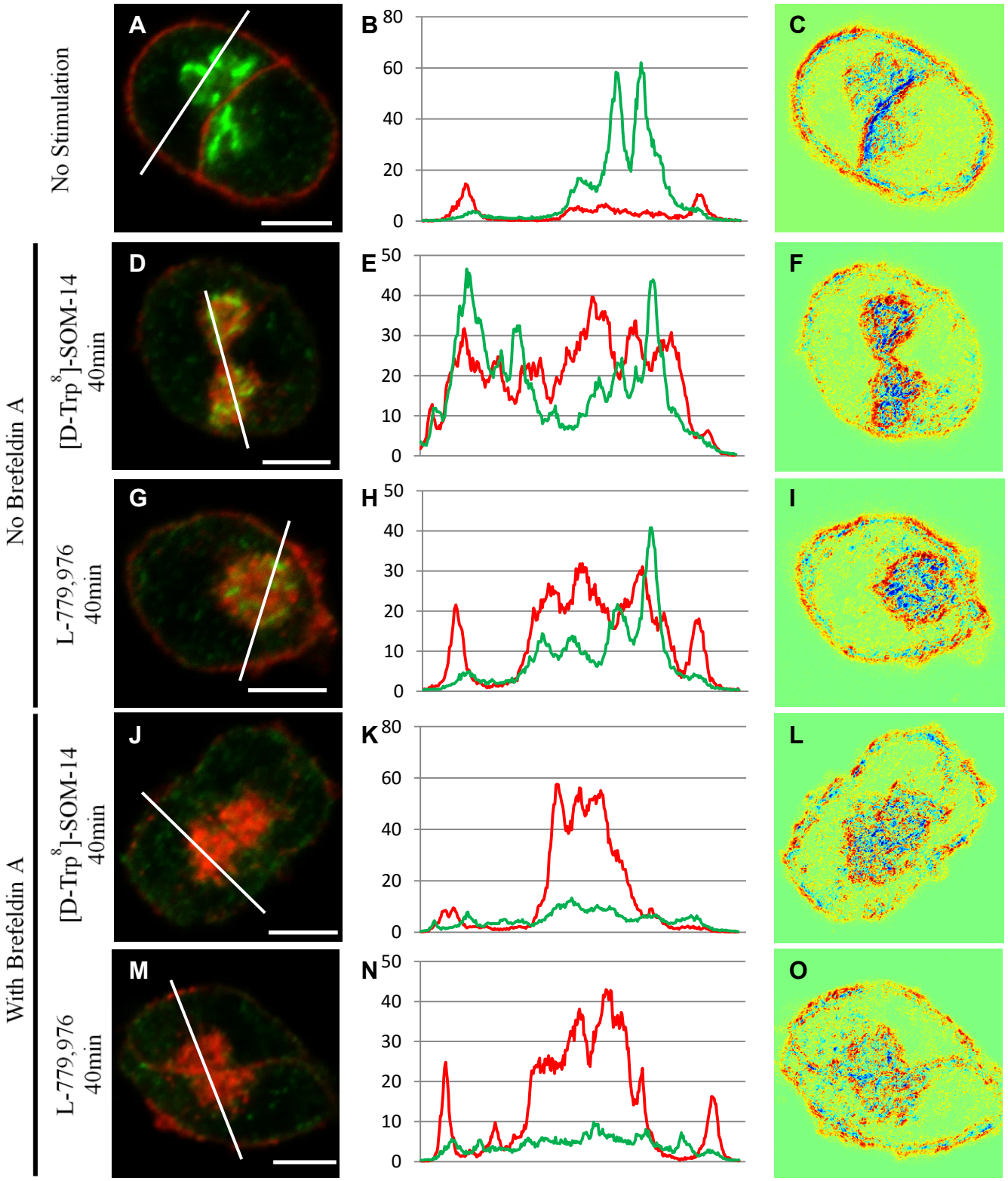

Fig 3.4: AtT-20 cells stimulated with L-779,976 or [D-Trp8]-SOM-14 for 40 min, with or without brefeldin A and immunostained for sst2A and PIST: Under baseline conditions, sst_{2A} is well segregated from PIST (A). Following stimulation with either agonists, sst_{2A} partially co-localizes with PIST (D,G), with fluorescence intensity profile analysis revealing that peaks of sst_{2A} occasionally align with peaks of PIST (E,H). Analysis by covarianceDetector reveals many regions where the two fluorescent signals are moving in opposing trends. When the TGN is disrupted by brefeldin A, PIST signal is entirely dispersed throughout the cytoplasm while sst_{2A} continues to internalize into the same perinuclear region (J,K,M,N), suggesting that a small portion sst_{2A} is sequestered in the TGN and most is localized to another compartment. N=4

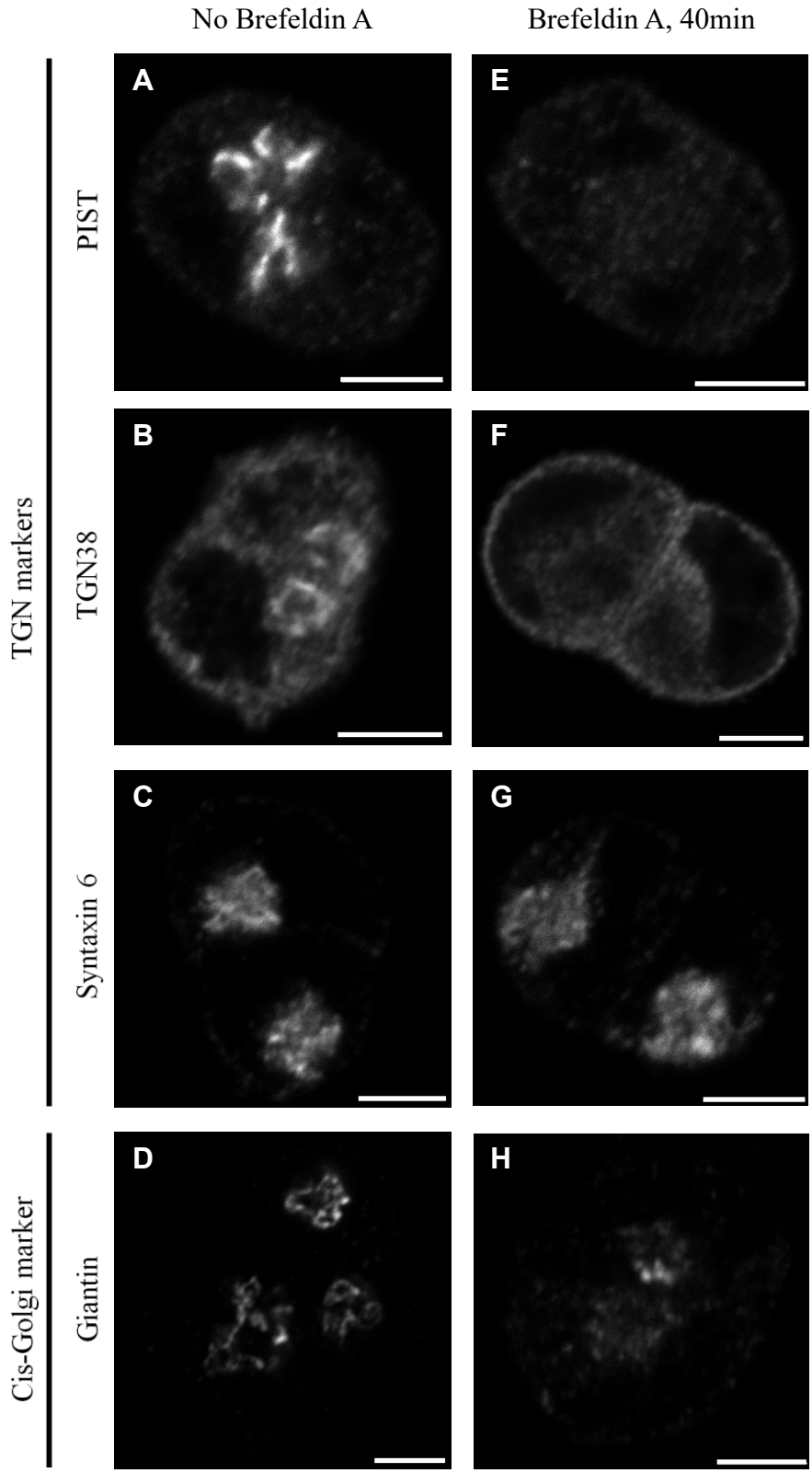

Fig 3.5 AtT-20 cells incubated with brefeldin A and stained for markers of the TGN and cis-Golgi: In the absence of brefeldin A, PIST, TGN38 and syntaxin 6 (all markers of the TGN) as well as giantin (cis-Golgi marker) label AtT-20 cells in their perinuclear region (A-D). With brefeldin A added, PIST and TGN38 labeling is completely dispersed (E,F). Giantin labeling is also greatly reduced (H), in keeping with the cis-Golgi merging with the endoplasmic reticulum. Surprisingly, syntaxin 6 labeling remained completely unaffected, remaining in the perinuclear region, suggesting that there is much syntaxin 6 outside the trans-Golgi network in AtT-20 cells.

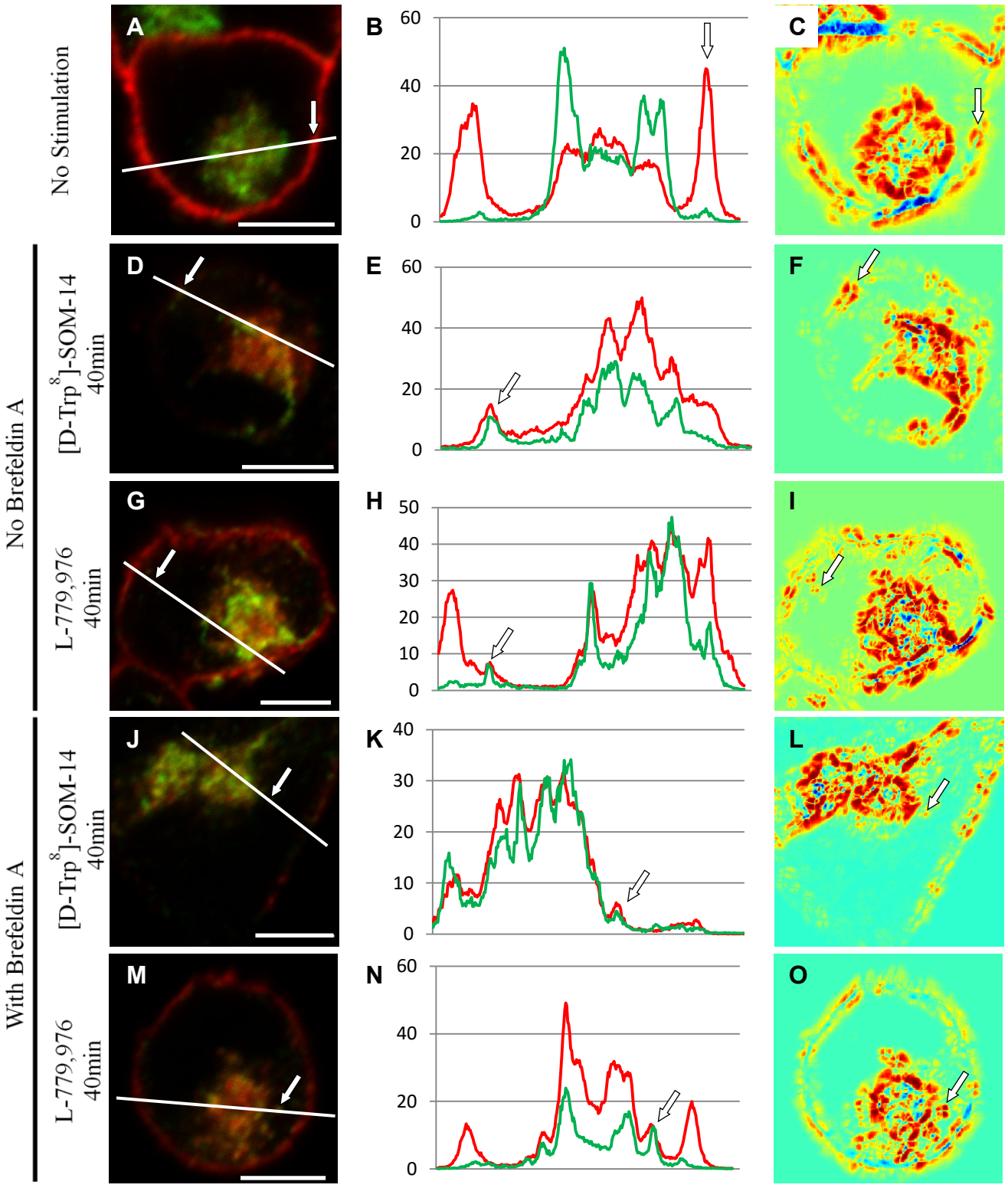

Fig 3.6: AtT-20 cells stimulated with L-779,976 or [D-Trp8]-som-14 for 40 min, with or without brefeldin A and immunostained for sst2A and Syntaxin 6: Internalized sst_{2A} following stimulation with either agonists co-localizes very well with syntaxin 6 (D,G,J,M), with fluorescent peaks for both proteins aligning very well in fluorescence intensity profile analyses (E,H,K,N). In covarianceDetector analysis, the perinuclear region is primarily red with very little blue, suggesting the two proteins co-vary very tightly (F,I,L,O). Sst_{2A} and syntaxin 6 co-localization occurs even with brefeldin A present, suggesting that the sst_{2A} outside the TGN is in the same compartment as syntaxin 6. The solid arrows show regions where covarianceDetector has detected sst_{2A} and syntaxin 6 co-localization at the plasma membrane and in the cytoplasm. N=4

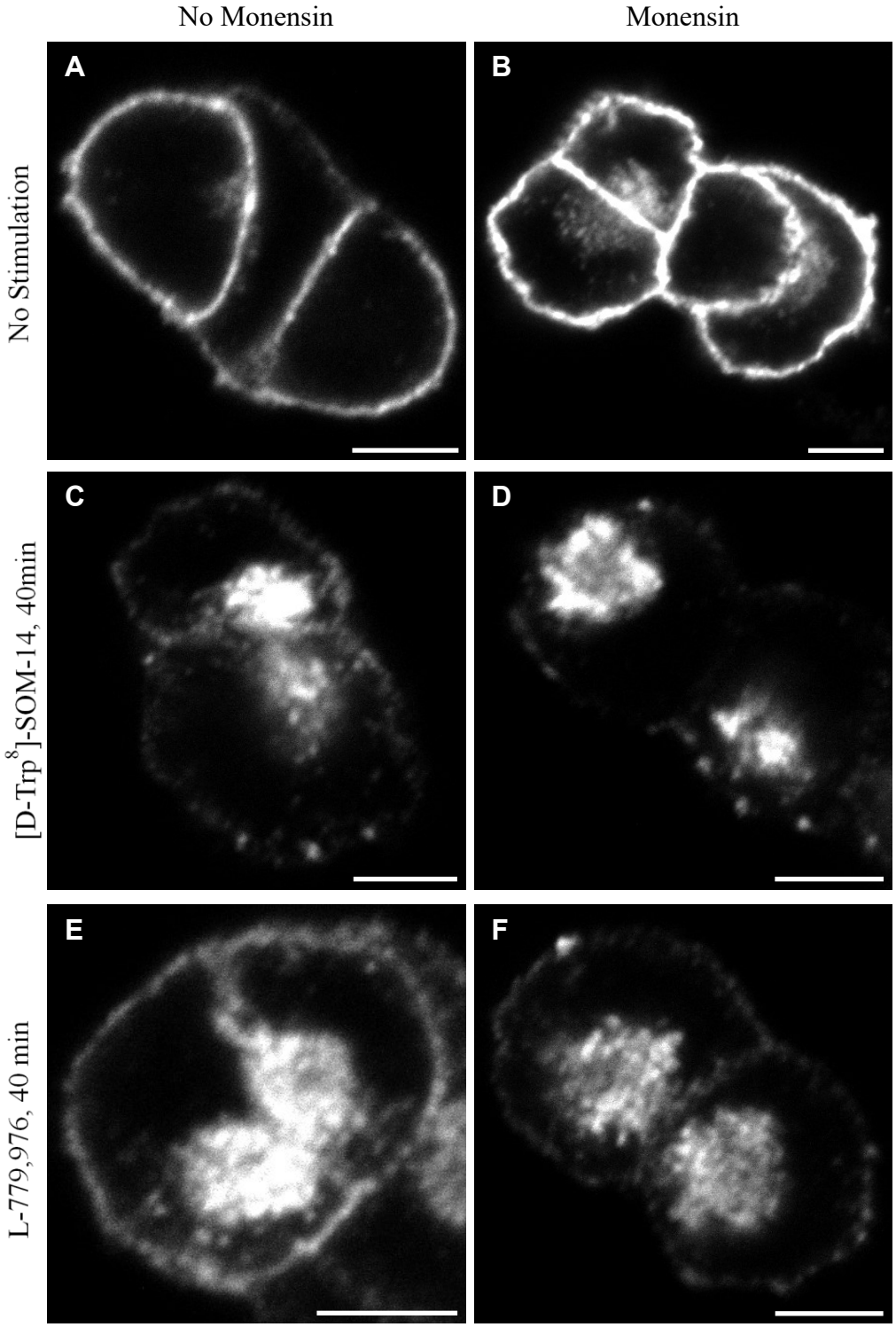

Fig 3.7: AtT-20 cells stimulated with [D-Trp8]-SOM-14 or L-779,976 in the presence of monensin, stained for sst2A: Sst_{2A} is localized to the plasma membrane under baseline conditions (A,B). After 40 minutes of stimulation with the non-selective agonist [D-Trp^{8}]-SOM-14, sst_{2A} internalizes completely, with or without the recycling inhibitor monensin (C,D). With the sst_{2A} selective agonist L-779,976, sst_{2A} internalizes to a perinuclear region, but maintains a presence at the plasma membrane (E). However, with monensin present, L-779,976 causes sst_{2A} to be internalized completely and abolishes any plasma membrane presence (F), suggesting that the presence of sst_{2A} at the plasma membrane with L-779,976 stimulation (E) is due to dynamic recycling of sst_{2A} after it internalizes. Scale bar = 5μm. N=3 Brightness increased by 20% in post-processing.

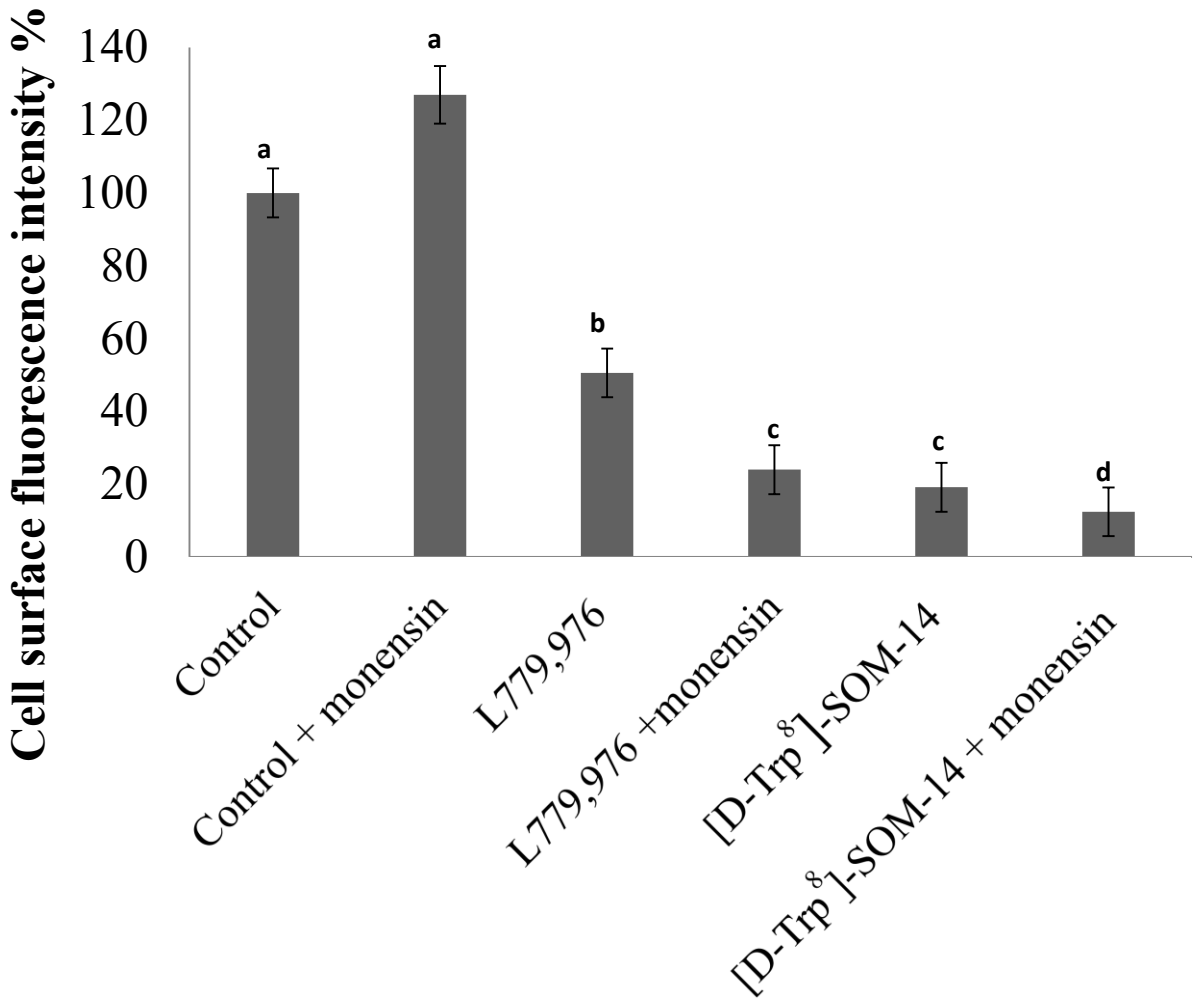

Fig 3.8 Quantification of surface fluorescence of sst2A in AtT-20 cells stimulated with [D-Trp8]-SOM-14 or L-779,976 in the presence of monensin: Bars not connected by a letter are statistically significantly different from each other. AtT-20 cells stimulated with L-779,976 are dimmer in peripheral fluorescence than unstimulated cells. When incubated with the recycling inhibitor monensin, L-779,976-stimulated cells lose their peripheral brightness and become indistinguishable from cells stimulated with [D-Trp^{8}]-SOM-14. Statistical significance calculated using a one-way ANOVA with Tukey's post-hoc comparison test with $p<0.05$. N=4

Chapter 4: Discussion

4.1 Primary Goal: Characterizing the Trafficking Pathway of sst_{2A}

4.1.1 Validating the Rab5 and Rab11 antibodies using Transferrin and determining co-localization

The use of Alexa647-transferrin as a third maker in these experiments was to validate the specificity of the Rab5 and Rab11 antibodies. Because Rab5 and 11 are constitutively expressed in all cells and fulfill critical functions (Stenmark 2009), knock out cell lines would most likely not be viable. It was therefore not possible to use that approach as a negative control for these antibodies. The transferrin receptor is known to internalize via clathrin coated, Rab5 positive vesicles (Bucci et al. 1992) and to recycle via the Rab11 pathway (Ullrich et al. 1996). Because transferrin remains attached to its receptor throughout the trafficking pathway (Gkouvatsos, Papanikolaou, and Pantopoulos 2012), fluorescently labeled transferrin applied to the cells simultaneously with agonist stimulation can be used as a positive control for the Rab5 and Rab11 antibodies. While not as robust as a knock out negative control test, our results nevertheless showed Alexa647-transferin co-localized with both Rab5 and Rab11, giving us more confidence in the signals produced by the two antibodies.

Profile analysis was used to determine whether the three proteins co-localized. A vesicle was considered "co-localized" for all three proteins if the fluorescence peaks for all three protein aligned in the same region. The relative intensities were considered less important: as long as a peak was clearly brighter than its background fluorescence levels, it was considered a peak.

The search for co-localization was usually performed visually. The covarianceDetector program was used in cases where visual analysis suggested that there was no co-localization analysis in order to automate a scan through every bright region in every image to find co-localization that would have otherwise been "missed." It was also used to investigate the

degree of covariance in regions that visually appear to be the site of co-localization as a 2D-extended version of a profile analysis.

4.1.2 Sst_{2A} internalizes via the Rab5 pathway and recycles via the Rab11 pathway

Sst_{2A} was shown to co-localize in cytoplasmic vesicles with Rab5 and Rab11 as well as transferrin.

Within one minute of stimulation with either agonist, sst_{2A} could be seen in cytoplasmic vesicles that were also immunofluorescently labeled Rab5 and Alexa647-conjugated transferrin. Such vesicles continued to be present up to 10 minutes following stimulation with both agonists, suggesting that sst_{2A} internalizes via the Rab5-positive, clathrin-coated vesicle pathway.

To investigate whether or not sst_{2A} recycled, experiments focussed on the L-779,976 agonist at the 40 minute time point, when recycling was expected to take place. Because some sst_{2A} vesicles were co-localized with transferrin but not Rab5, it suggested that sst_{2A} recycled via the same pathway as transferrin, namely, the Rab11 pathway (Ullrich et al. 1996). Rab11 was therefore chosen over Rab4 as the recycling pathway to investigate.

Fluorescent imaging consistently revealed that sst_{2A} was distinctly co-localized in vesicles containing Rab11 and transferrin, suggesting that sst_{2A} recycles via the Rab11 pathway.

4.1.3 Sst_{2A} is not targeted towards the Rab9 degradative pathway following internalization

Some GPCRs are targeted for degradation following internalization. To investigate whether or not this was the case for sst_{2A}, AtT-20 cells were stained for sst_{2A} and Rab9.

Upon visual analysis, sst_{2A} and Rab9 seemed very well segregated. Rab9 staining was punctate and distributed throughout the cytoplasm while sst_{2A} staining was either at the plasma

membrane under baseline conditions or within the perinuclear region when stimulated with either agonist. Upon profile analysis, the Rab9 vesicles all seemed to be void of any sst_{2A}.

In the rare instances where Rab9 labeling seemed to coincide with sst_{2A} labeling, the rise in Rab9 immunostaining was typically accompanied by a constant level of sst_{2A} immunostaining at the plasma membrane or in many cases, with a local decrease in sst_{2A} labeling, seen in the plasma membrane of unstimulated cells or even within the perinuclear build-up of sst_{2A} in stimulated cells, suggesting sst_{2A} and Rab9 are not co-localized.

However, to "prove" that sst_{2A} and Rab9 never co-localized would have required verifying every single Rab9 vesicle to check for an even weak sst_{2A} presence. This process would be prohibitively time consuming to do by hand. Thus, the sets of images were analyzed by covarianceDetector.

On very rare occasions, covarianceDetector flagged regions in red that it interpreted as sites of co-localization of sst_{2A} with Rab9. A profile analysis of such regions revealed that they were indeed instances where sst_{2A} and Rab9 peak together. However, these events were very rare, occurring once in several cells and did not change in frequency between baseline and stimulated conditions. This suggests that while sst_{2A} may get degraded, it isn't actively targeted for degradation following stimulation and internalization.

4.1.4 sst_{2A} is partially co-localized to the Trans-Golgi Network in AtT-20 cells

In order to determine the intracellular compartment into which sst_{2A} was internalized, AtT-20 cells were stimulated with [D-Trp^8]-SOM-14 and L-779,976 with or without the TGN disruptor brefeldin A and stained for various markers of the TGN. It was found that sst_{2A} only partially co-localized the TGN marker PIST. In cells incubated in brefeldin A, PIST labeling was

dispersed through the cytoplasm, but sst_{2A} was insensitive to brefeldin A and continued to be sequestered in the perinuclear region. A pilot experiment confirmed that brefeldin A was working normally, disrupting not only PIST labeling but also TGN38 and even giantin labeling. However, one supposed marker of the TGN, syntaxin 6 was also insensitive to brefeldin A action and in colabeling experiments, was found to co-localize almost perfectly with internalized sst_{2A} not only in the perinuclear region but also in vesicles at the plasma membrane and cytoplasm. This suggests that in AtT-20 cells, sst_{2A} does not internalize into the TGN, but is instead sequestered in another, as yet unknown but syntaxin 6-positive compartment.

Internalized sst_{2A} was found to only partially co-localize with the TGN marker PIST. Visually, fluorescence from both signals was present within the perinuclear region. However, a fluorescence intensity profile analysis across the perinuclear region revealed that peaks of sst_{2A} and PIST immunoreactivity only occasionally aligned. Very often, peaks in one channel actually aligned with troughs in the other. Visualized using covarianceDetector, the perinuclear region in stimulated cells was painted with a very large amount of dark blue, meaning that immunoreactivity in the two channels often moved in opposing trends.

When the stimulation and staining experiments were repeated in cells incubated with brefeldin A, a drug that disrupts the TGN, perinuclear PIST fluorescence was completely disrupted by brefeldin A. However, there was no visible difference in the sst_{2A} fluorescence patterns.

These results were unexpected; previous literature indicated that internalized sst_{2A} should be localized exclusively in the TGN. The partial co-localization of sst_{2A} and PIST shows that there is sst_{2A} within the TGN, but it also suggests the existence of a second compartment. The

brefeldin A incubation experiment confirmed this suspicion and indicates that this second compartment can be distinguished from the TGN through its brefeldin A-insensitivity. While the ratio was not quantified in these experiments, the fact that there was no visible difference between perinuclear sst_{2A} fluorescence with or without brefeldin A suggests that the amount of sst_{2A} that was contained within the TGN and that would have been dispersed by brefeldin A is in fact quite small in comparison to the amount contained outside the TGN.

4.1.5 Syntaxin 6 labels a perinuclear compartment that is not the trans-Golgi network

Because of the unexpected nature of these results, the efficacy of brefeldin A was tested by incubating cells with brefeldin A and staining them for other markers of the Golgi apparatus, three TGN markers: PIST, TGN38 and syntaxin 6 along with a cis-Golgi cisterna marker: giantin. With brefeldin A, PIST and TGN38 immunofluroescent labeling was completely dispersed as expected and giantin fluorescent labeling too was strongly weakened, corresponding to the expected effect of TGN disruption and cis-Golgi cisternae merging with the endoplasmic reticulum (Sciaky et al. 1997).

Surprisingly, the third TGN marker, syntaxin 6, was completely unaffected by incubation with brefeldin A and remained concentrated in the perinuclear region. Furthermore, a co-localization experiment between PIST and syntaxin 6 showed partial co-localization of the two proteins, with much syntaxin 6 labeling occurring outside regions that were positive for PIST. This suggests that, in AtT-20 cells at least, syntaxin 6 is not a marker for the TGN because while a small portion of syntaxin 6 is located within the TGN, the majority of it is instead localized in an unknown, brefeldin A-insensitive compartment.

4.1.6 Intracellular sst_{2A} not present in the TGN is localized in a syntaxin 6-positive, brefeldin A-insensitive unknown compartment

To investigate whether or not sst_{2A} and syntaxin 6 were in fact stored within the same compartment, Att-20 cells were stimulated with either [D-Trp^8]-SOM-14 or L-779,976 in the presence or absence of brefeldin A. Internalized sst_{2A} co-localized near perfectly with syntaxin 6 within the perinuclear region. A fluorescence intensity profile analysis across the perinuclear region showed that unlike sst_{2A} and PIST colabeling, peaks of sst_{2A} almost always aligned with peaks of syntaxin 6. An analysis by covarianceDetector reveals that the perinuclear region is painted primarily in large, continuous clouds of red with minimal blue, suggesting that the two channels are increasing and decreasing together (covarying) very tightly in this region.

This suggests that within the perinuclear region, the fraction of sst_{2A} that is not localized within the TGN is contained within the same, brefeldin A-insensitive subcellular compartment as syntaxin 6. The identity of this compartment remains unknown.

4.1.7 covarianceDetector shows sst_{2A} and syntaxin 6 co-localization in the cellular periphery

When the sst_{2A} and syntaxin 6 colabeled cells were analyzed by covarianceDetector, the software also reported co-localization at the plasma membrane and cytoplasm in addition to the perinuclear region. In fact, this type of weak, but distinct co-localization can be found in all stimulated conditions. Furthermore, syntaxin 6 could also be found co-localized with sst_{2A} at the plasma membrane under control conditions. This suggests that syntaxin 6 begins to interact with sst_{2A} much sooner than within the perinuclear region and may even play a role in its internalization. Alternatively, it could also suggest a role of syntaxin 6 in the recycling of sst_{2A}.

4.2 Secondary Goal: Pharmacological Investigation of sst_2 Recycling

Monensin's ability to abolish the presence of sst_{2A} at the plasma membrane in AtT-20 cells stimulated with L-779,976 suggests that sst_{2A} recycles to the plasma membrane. It also suggests that sst_{2A} intracellular trafficking must pass through the Golgi apparatus.

Monensin is an inhibitor of exocytosis. Its presence abolishes the presence of sst_{2A} at the plasma membrane in AtT-20 cells following stimulation with L-779,976. Because monensin works by inhibiting recycling, this is a very strong indication that the recycling of sst_{2A} is necessary for the maintenance of sst_{2A} following L-779,976 stimulation.

The inhibition of recycling by monensin also suggests that sst_{2A} intracellular trafficking must pass through the Golgi apparatus. Monensin is known to primarily act at the Golgi apparatus. In fact, its mode of action is sufficiently well established in the literature that its ability to inhibit recycling of a protein is typically interpreted as a strong sign that the protein in question must traverse the Golgi apparatus (Mollenhauer, James Morré, and Rowe 1990).

4.3 Questions and Future Directions

The results obtained indicate that sst_{2A} stimulated by L-779,976 in AtT-20 cells is internalized before being recycled back to the plasma membrane. However, several questions remain unanswered.

4.3.1 The monensin and the Golgi buildup of trafficking

The first one concerns a discrepancy the previous known effects of monensin and the sst_{2A} intracellular build-up determined in the current set of experiments. Monensin is known to act at the Golgi apparatus and indeed, it is used as a test to determine whether or not the trafficking of a protein traverses the Golgi apparatus. And yet, sst_{2A} co-localization experiments

performed here show that even without any pharmacological modifications, sst_{2A} is localized primarily in a syntaxin 6 positive compartment that is not the trans-Golgi network.

One way to resolve this paradox is to propose that the syntaxin compartment sits upstream of the TGN in the sst_{2A} trafficking pathway and that it may act as a storage buffer that prevents overwhelming of the TGN.

If this were the case, it would suggest that the intracellular build-up of sst_{2A} in the monensin experiments may be fundamentally different from build-up of sst_{2A} under stimulation conditions. The first would occur within the Golgi apparatus while the second, as we saw through co-localization experiments, occurs within syntaxin 6 compartments. To test this, cells should be pre-incubated with monensin, stimulated with both agonists for 40 minutes and then stained for sst_{2A} combined with PIST or syntaxin 6. If this model is correct, then the co-localization preference of sst_{2A} should switch from syntaxin 6 to PIST in the presence of monensin.

A second experiment that could be performed if that first experiment proves correct is a double pharmacological experiment. Cells should be incubated with monensin and then stimulated for 40 minutes. Brefeldin A should then be applied to the cells for 20 minutes to disrupt the Golgi apparatus, which, in theory, should be the buildup site of sst_{2A} under these conditions. If the addition of Brefeldin A under these conditions does disperse the perinuclear labeling of sst_{2A}, then it would be a strong line of evidence suggesting that sst_{2A} does enter the Golgi apparatus, but after passing through the syntaxin 6 "buffer zone."

This model could also explain why sst_{2A} seems to co-localize so little with PIST and the TGN. If sst_{2A} is indeed stored within the syntaxin 6 compartment buffer zone as it is more slowly

imported into the TGN for sorting and recycling, then it would be normal that sst_{2A} co-localize overwhelmingly with syntaxin 6 and very little with PIST. A pilot experiment performed colabeling sst_{2A} cells for PIST and syntaxin 6 (data not shown) revealed a labeling pattern somewhat similar to that of PIST and sst_{2A}: mostly distinct with some overlapping regions. This could suggest that some of the syntaxin 6 compartment merges with the PIST containing TGN as sst_{2A} moves from the former to the latter.

Finally, a third experiment that could test this linearity of this "buffer zone" model of sst_{2A} is simply to perform a periphery brightness analysis of surface L-779,976 in AtT-20 cells incubated with brefeldin A. In principle, brefeldin A should block the net recycling of sst_{2A} as well as monensin and so, surface brightness should be equivalent. An early pilot analysis places the surface brightness of sst_{2A} in L-779,976 with brefeldin A at approximately 40% of control, which is between L-779,976 (50%) alone and L-779,976 with monensin (30%). Statistical significance has not yet been calculated. However, if L-779,976 turns out to be statistically significantly brighter than L-779,976 with monensin, it may suggest that an alternative recycling pathway may be used in the brefeldin A condition. One possibility is that the syntaxin 6 compartment may be a form of sorting endosomes, which opens the possibility of sst_{2A} recycling via the Rab4 pathway.

4.3.2 Question 2: The nature of the syntaxin 6 positive compartment

While a model was just proposed in the previous section, the fact remains that there are very few indicators of what the non-TGN, syntaxin 6-positive compartment could be. Syntaxin 6 is primarily known as a marker for TGN and these experiments have clearly shown that, in AtT-20 cells at least, that is not necessarily the case.

Considering it is the buildup site for a receptor that was just internalized, it may be tempting to think that this compartment is a sorting endosome. One way to test this would be to colabel syntaxin 6 with Rab4 and Rab11, which are both present on sorting endosomes.

This technique of colabeling for "suspected" markers, however, is a bit "hit-and-miss." If it proves to be correct, it would be a lucky shot and if not, it would provide very little recourse to identify the compartment. Instead, another strategy is proposed the following section in the context of another question.

4.3.3 Question 3: Identifying the interaction partners of sst_{2A}

While syntaxin 6 co-localizes very well with sst_{2A}, it remains a t-SNARE. Thus, while it is an excellent marker for the compartment in which sst_{2A} is present, it is itself unlikely to be the interaction partner that anchors sst_{2A} to that compartment. An important future goal is to identify the interaction partners of sst_{2A} as it is trafficked through the cell: whether it is chaperoned across multiple compartments with one particular binding partner or handed off across several interaction partners.

Because sst_{2A} is so concentrated in syntaxin 6 compartments, one strategy is to perform a subcellular fraction for that compartment. Out of the remaining pool of proteins, interaction partners of sst_{2A} can be identified by performing a co-immunoprecipitation experiment. The isolated proteins can be then be identified by mass spectrometry.

This approach can also lend itself to the identification of the syntaxin 6 positive compartment. If the pool of proteins co-immunoprecipitated with sst_{2A} does not contain any markers for an intracellular compartment, then the range of proteins analyzed by mass spectrometry can be broadened by skipping the sst_{2A} co-immunoprecipitation step and

proceeding directly to mass spectrometry following purification of the proteins contained within the subcellular fraction. One would then look for proteins that are compartment markers.

4.3.4 Question 4: The role of somatostatin receptor 5 in somatostatin receptor 2 trafficking

It is important to keep in mind that the fast recycling of sst_{2A} within AtT-20 cells is dependent on the presence of unstimulated sst_5. Indeed, L-779,976 exerts an agonistic action exclusively on sst_{2A} while leaving sst_5 unstimulated. This effect is not due to L-779,976 and [D-Trp^8]-SOM-14 having different effects on sst_{2A} either. In CHO cells stably transfected with sst_{2A} only and stimulated with L-779,976, sst_{2A} was internalized and did not maintain a presence at the plasma membrane while in CHO cells stably transfected with both sst_{2A} and sst_5, L-779,976 stimulation yielded the same phenotype observed in AtT-20 cells: sst_{2A} maintained at the plasma membrane (Sharif et al. 2007).

However, the CHO cell remains an exogenous expression model. To investigate the role of sst_5 in sst_{2A} trafficking, it is important to perform an experiment equivalent to the CHO_{sst2A} experiment in the AtT-20 cells which endogenous express both receptors. One strategy would be knock out the sst_5 gene from AtT-20 cells and stimulate these AtT-20_{sst5KO} cells with both agonists and see if sst_{2A} fails to recycles to the plasma membrane upon L-779,976 stimulation. It would be then interesting the repeat the range of experiments performed here and see if sst_{2A} switches cellular compartment in the absence of sst_5.

4.3.5 covarianceDetector compared to other analysis methods

covarianceDetector is a prototypical piece of software designed to automate the detection of co-localization sites and report them to the investigator for further manual analysis.

covarianceDetector works on a fundamentally different principle than pre-existing co-localization software which are based either the Pearson correlation coefficient (PCC) or the Mander's co-localization coefficient (MCC). These measures give a global measure of the correlation between the two channels. covarianceDetector takes an entirely different approach to detecting co-localization. It interprets each pixel in the context of its environment. Each pixel in each channel is part of a region that possesses a trend in brightness, whether it be increasing, decreasing or holding steady. By considering whether the region is increasing or decreasing in brightness and in what orientation across both channels, the similarity in trends across both channels can be assessed and painted on a heatmap. If a pixel is part of a rising or decreasing trend in brightness in both channels, it is painted in increasingly warm colours (yellow, orange and red). If by contrast, it is part of an increasing trend in one channel but a decreasing one in the other, it will be painted in shades of blue. The concept is not yet validated, but in the course of this project, has demonstrated itself to possess some benefits over other analysis methods, but some drawbacks as well.

Co-localization is a very physical phenomenon that happens in distinct regions. Ironically, most analyses methods seem to struggle with finding those regions. The main benefit of covarianceDetector is that it is designed from the ground up to detect the location of co-localization. While PCC based systems are good to calculate if the image, overall, has a trend for bright pixels to correlate with each other, they usually struggle to report where co-localization takes place and when they do, the results do not always have biological meaning. What PCC-based systems do to map co-localization is to generate a scatter plot and then highlight a square within it and reports the location of the pixels contained within that region of the scatterplot in the original images. In other words, the criteria such an implementation uses to

highlight pixels in the image is “if a pixel’s brightness in one channels falls within a certain range and if its brightness in the other channel also falls within a certain range then highlight it.” This is very easy to implement in programming, but upon reflection, possess very little biological meaning. A pixel whose brightness falls within the selected range in both channels may sit at the tip of a peak of fluorescence intensity in one channel but at the centre of the trough in the other channel. By contrast, covarianceDetector is specifically designed to consider such scenarios where the trend in brightness makes a big difference. It does so by considering each pixel in each channel in the context of its environment and paints it red or blue depending on whether the trends are moving in the same or opposing directions. The resulting heatmap given to the user reports these trends with very high spacial resolution.

The second benefit of covarianceDetector is that it is capable of detecting co-localization in conditions that would be challenging for PCC based system, such as co-localization in a very dim area or co-localization where one channel vastly outshines the other, especially if the image possesses many regions where both channels do co-localize brightly. In the first scenario, pixels dim in both channels would be located near the bottom left region of the scatterplot. Their presence would entirely be masked by a cloud of other dim pixels and while they may contribute to the computation of the PCC value, they cannot be highlighted by PCC-based localization techniques since highlighting the bottom left region of the scatterplot would highlight too many dark pixels to find the ones actually contributing to co-localization, assuming the investigator even suspects they exist in the first place. By contrast, covarianceDetector considers each pixel in its local context and so, even dim sites of covariance will be highlighted in red. In the other scenario where one channel vastly outshines the other, it may be possible for PCC-based localization techniques to identify them if there are enough such pixels to form a second, visible,

narrow point-cloud distinct from the main trend. However, this is only possible if there is a large amount of such pixels, a subpopulation of significant size. If instead, such events are very rare, then the points they create on the scatterplot may be too diffuse to draw the attention of an investigator. Again, because covarianceDetector looks for *local* trends in brightness shift, such regions can be highlighted in red.

The third benefit of covarianceDetector is its capability to report antivariance at very specific locations. In principle, negative PCC values can also report anti-correlation, but realistically, fluorescent images are extremely unlikely to give negative PCC's. This is because fluorescent images have more black pixels (background) than bright pixels. Even if ROIs are selected, pixel brightness will range from dim to dark and again, with more dark pixels than bright ones. As such, scatterplots almost always have a cluster of very dark pixels at their bottom left corner. In generating a line of best fit through all pixels, this cluster will almost always ensure that the line starts near the (0,0) intersect. For a scatterplot to have a negative PCC, the line of best fit would need to start near the top left corner and move towards the lower right corner. For an image to generate this kind of trend, every pixel not filled by one channel necessarily has to be filled by the other, which simply isn't the case in fluorescence imaging. Yet antivariance *does* occur within the images. Only it does so in discrete regions and is not common enough to shift the entire PCC towards a negative value. covarianceDetector, on the other hand, is designed to reveal these regions because it observes local trends in brightness change.

However, covarianceDetector remains a prototype and still possesses several pitfalls and shortcomings. First, while the idea of detecting covariance is good in principle, the implementation has a tendency of creating noisy images. Low-pass filtering images helps with that regard, but the more aggressively that is done, the more finer features in the cell will be lost.

The second problem is that it has a tendency to report false positives. covarianceDetector reports covariance, not co-localization. As such, certain patterns of fluorescence cause covarianceDetector to paint a region in red, which may mislead the investigator into thinking there is co-localization present. For example, the edges of cells will frequently be painted in red because both channels are increasing together at that region. But they are increasing, not necessarily because there is co-localization, but because the image is shifting from the background of the coverslip to the background of the cytoplasm in both channels. As such, regions in red must always be confirmed by a manual fluorescence intensity profile analysis of the region. Ironically, this tendency to report false-positives rather than false-negatives may make covarianceDetector well suited as a tool for confirming any lack of co-localization, as was used in this project for sst_{2A} and Rab9 co-localization.

A third shortcoming of covarianceDetector is tied to its analysis method: it is not a quantitative tool. For all its flaws, PCCs allow for easy comparison between images. covarianceDetector can only return two heatmaps and direct comparison beyond a visual sense of "more red in this image" is difficult. It would be easy to sum up the total score of each pixel in the heatmap to get a net score to determine whether an image contains more covariance or antivariance. However, whether such a number would have any biological meaning is not yet known.

covarianceDetector cannot and was not meant to replace co-localization analysis by PCC. Its intended use is as a targeting system for manual analysis and to that end, it fulfills its purpose well. It will require further testing in various conditions and further validation before it is ready for wider release if its conributions are considered useful. Two general goals are set.

The first is to run it through a battery of artificial but mathematically well-defined images and observe its behaviour. For example one test would consist of a pair of sine-wave gratings with various offsets in order to investigate how covarianceDetector behaves with misaligned peaks. Early tests with AtT-20 cells stained for sst_{2A} and SHANK reveal that slightly offset peaks produces a very distinctive sandwich of red-blue-red labeling at the plasma membrane (Supplemental Fig 2). Whether this pattern can be used as an indicator of offset peaks will depend on whether other patterns can also cause covarianceDetector to display this pattern.

The second general goal is to see if covarianceDetector can be paired with statistical methods. For example, it is conceivable to use covarianceDetector to highlight both regions of covariance and antivariance and analyze these as regions of interests in a PCC analysis. In principle, the highlighted regions detected by covarianceDetector should yield very high PCCs for the red regions and very negative PCCs for the blue regions. Automated ROI generating techniques for PCC analyses already exist, such as the Coste's automatic thresholding method. However, that method is, in essence, a high-pass filter that removes broad features from the image by subtracting a certain brightness value from every pixel. Thresholding, however, always bears the risk of losing data. It would very interesting to investigate whether the ROIs defined by covarianceDetector and Coste's automatic thresholding method yield different PCCs.

covarianceDetector also needs to be further developed to make it a more robust analysis method. Currently, covarianceDetector has only been used on 1024x1024 pixel images with a bit-depth of 8. Trials on 16-bit images create images extremely grainy images with yellow regions in the 8-bit heatmap appearing in red (Suppl. Fig 3B&C). The reason for this stems from the values encoding the gray values. In an 8-bit image, white is represented by 254 while in a 16-bit image, white is represented by 65535. The consequence of this is that in the 16-bit image,

any feature in the images rises by 256 times more brightness values over the same distance across the XY plane than it would have in an 8-bit image. In other words, any change in brightness appears much more intense. This not only boosts the score given by the comparatorSlaved module as all normal vectors are now squeezed closer together towards the horizontal plane (Suppl. Fig 3D&E) but also increases the interest score given by cosWeighterSlaved because the normal vectors are, again, closer to the horizontal plane. Other such run-time bugs must be identified and rectified prior to a possible general release.

The goal for covarianceDetector is further validation and testing under various conditions and ultimately, if the output it generates is judged to be of sufficient use to investigators, it may be converted from its current MatLab® form into a plugin for ImageJ.

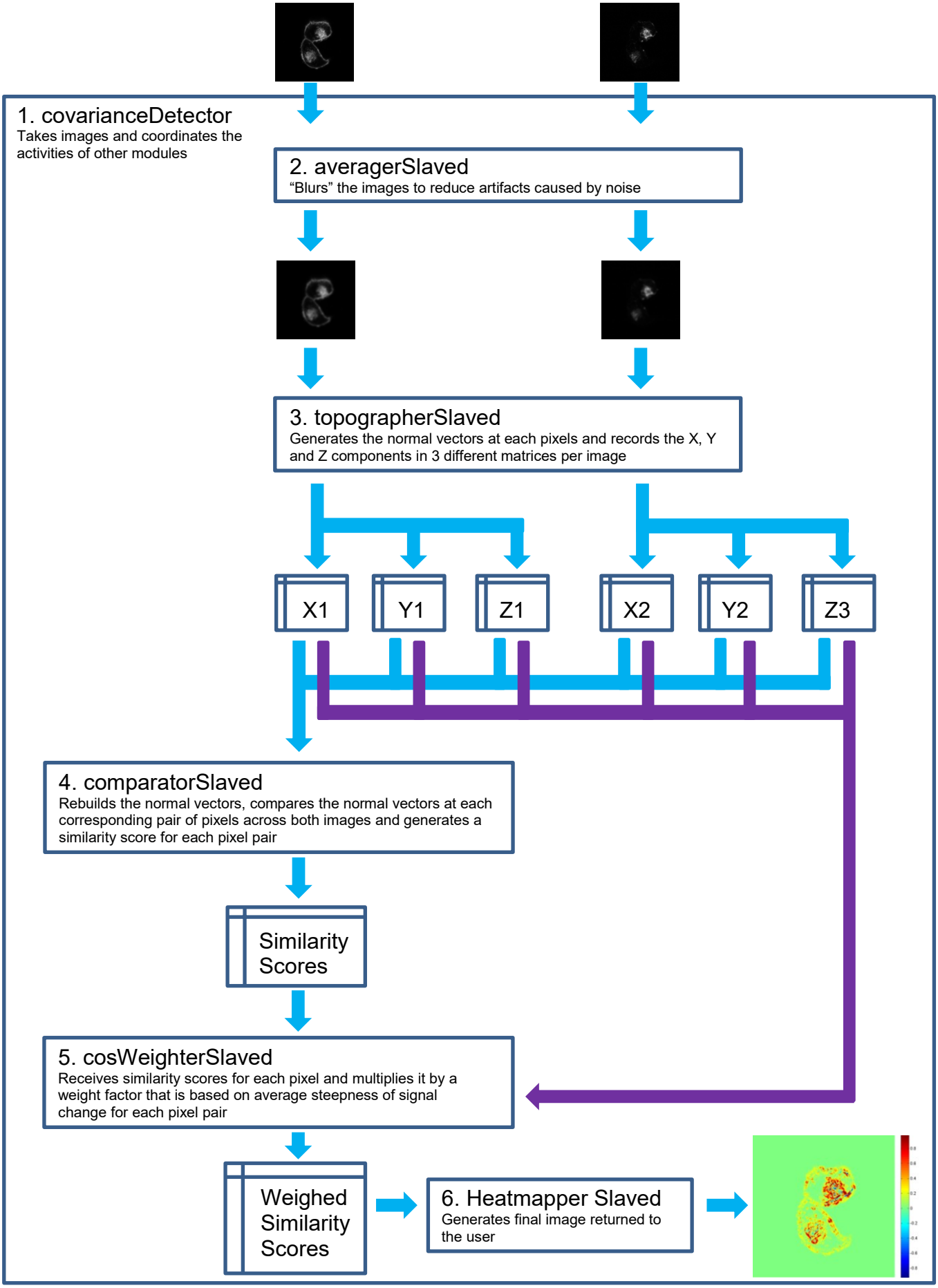

Supplemental Figure 1: Schematic representation of covarianceDetector Function

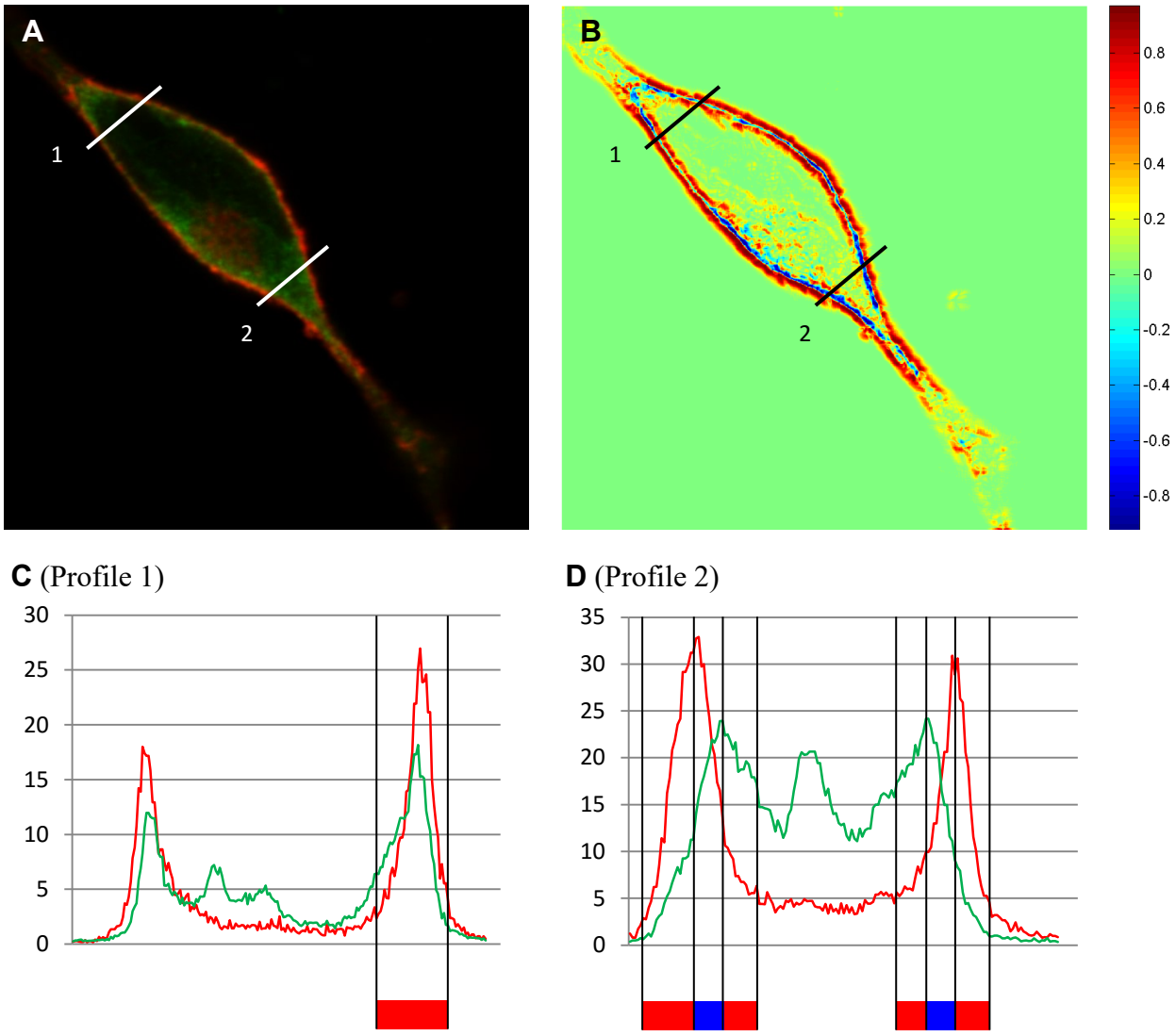

Supplemental Figure 2: covarianceDetector shows a red-blue-red pattern when peaks of sst_{2A} and Shank are slightly offset

When two peaks are slightly offset (trace 2), covarianceDetector creates a characteristic red-blue-red band pattern. The blue region is created by the region between the two peaks where the two channels are moving in opposing directions. Whether this can be considered a pattern useful for analysis or an artifact depends on how distinctive this pattern is in other situations.

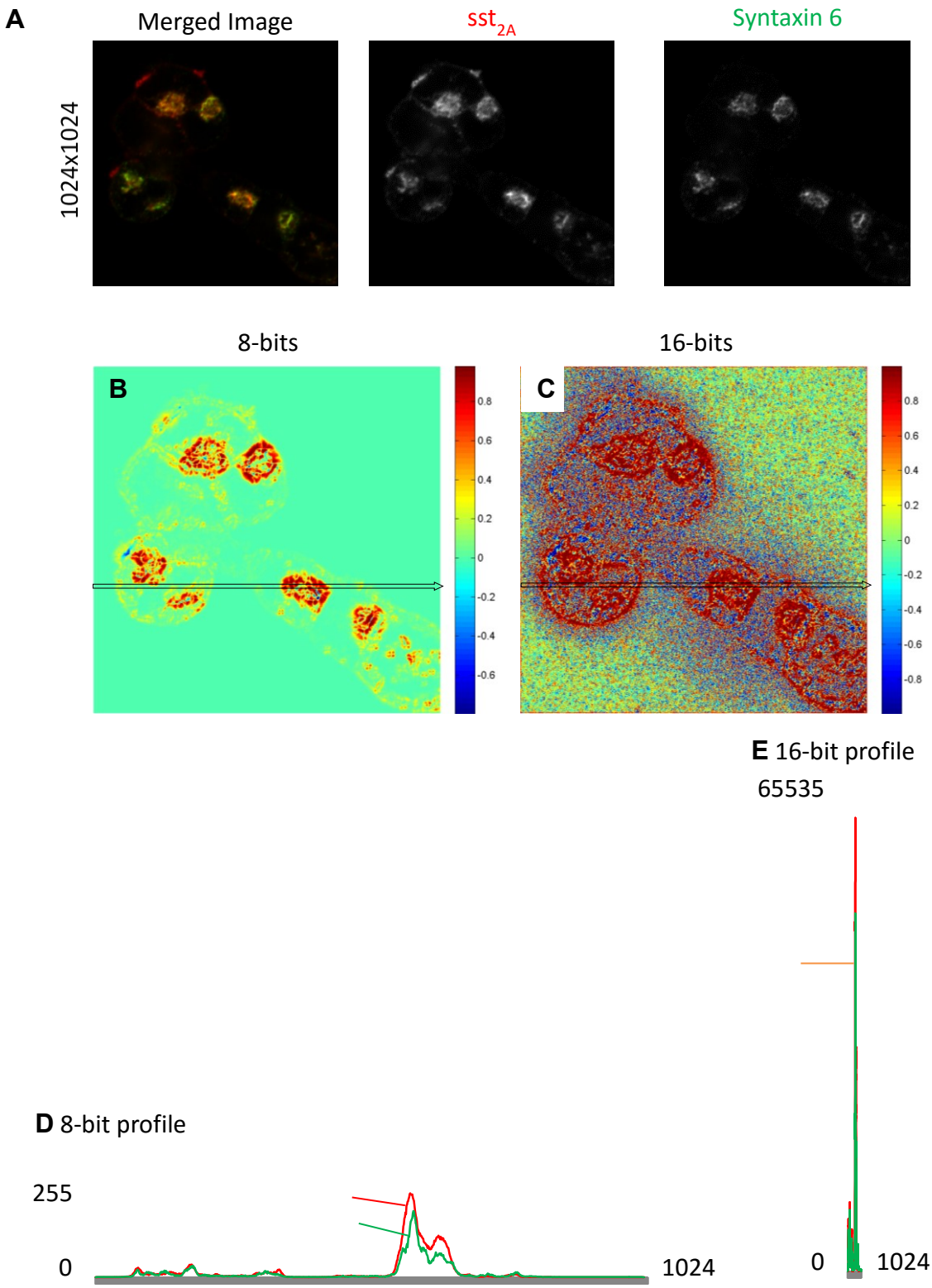

Supplemental Figure 3: The use of 16-bit grayscale images increases the noise present in the heat-map and artificially increases covariance scores, resulting in more red regions

The same shade of gray in a 16-bit image is encoded by a number 256 times higher than the same shade in an 8-bit image. Thus, features in 16-bit images create far more horizontal normal vectors than in 8-bit images. This boosts the covariance score as both normal vectors are pushed closer together to the horizontal while also boosting cos weight score, which is why 16-bit images have far more red regions than 8-bit images.

Chapter 5: Bibliography

Alberti, K. G. M. M., N. Juel Christensen, S. Engkjær Christensen, A. A. Prange Hansen, J. Iversen, K. Lundbæk, K. Seyer-Hansen, and H. rskov. 1973. 'Inhibition of Insulin Secretion by Somatostatin', *The Lancet*, 302: 1299-301.

Anborgh, Pieter H., Jennifer L. Seachrist, Lianne B. Dale, and Stephen S. G. Ferguson. 2000. 'Receptor/β-Arrestin Complex Formation and the Differential Trafficking and Resensitization ofβ 2-Adrenergic and Angiotensin II Type 1A Receptors', *Mol Endocrinol*, 14: 2040-53.

Bauer, Wilfried, Ulrich Briner, Wolfgang Doepfner, Roland Haller, René Huguenin, Peter Marbach, Trevor J. Petcher, and Janos Pless. 1982. 'SMS 201–995: A very potent and selective octapeptide analogue of somatostatin with prolonged action', *Life Sciences*, 31: 1133-40.

Ben-Shlomo, A., and S. Melmed. 2010. 'Pituitary somatostatin receptor signaling', *Trends Endocrinol Metab*, 21: 123-33.

Ben-Shlomo, Anat, and Shlomo Melmed. 2008. 'Somatostatin agonists for treatment of acromegaly', *Mol Cell Endocrinol*, 286: 192-98.

Ben-Shlomo, Anat, Herbert Schmid, Kolja Wawrowsky, Oxana Pichurin, Erika Hubina, Vera Chesnokova, Ning-Ai Liu, Michael Culler, and Shlomo Melmed. 2009. 'Differential Ligand-Mediated Pituitary Somatostatin Receptor Subtype Signaling: Implications for Corticotroph Tumor Therapy', *The Journal of Clinical Endocrinology & Metabolism*, 94: 4342-50.

Benovic, J L, H Kühn, I Weyand, J Codina, M G Caron, and R J Lefkowitz. 1987. 'Functional desensitization of the isolated beta-adrenergic receptor by the beta-adrenergic receptor kinase: potential role of an analog of the retinal protein arrestin (48-kDa protein)', *Proceedings of the National Academy of Sciences*, 84: 8879-82.

Bevan, John S. 2005. 'The Antitumoral Effects of Somatostatin Analog Therapy in Acromegaly', *The Journal of Clinical Endocrinology & Metabolism*, 90: 1856-63.

Bilezikjian, Louise M., and Wylie W. Vale. 1983. 'Stimulation of Adenosine 3',5'-Monophosphate Production by Growth Hormone-Releasing Factor and Its Inhibition by Somatostatin in Anterior Pituitary Cells in Vitro', *Endocrinology*, 113: 1726-31.

Binaschi, A., G. Bregola, and M. Simonato. 2003. 'On the role of somatostatin in seizure control: clues from the hippocampus', *Rev Neurosci*, 14: 285-301.

Bock, J. B., J. Klumperman, S. Davanger, and R. H. Scheller. 1997. 'Syntaxin 6 functions in trans-Golgi network vesicle trafficking', *Molecular Biology of the Cell*, 8: 1261-71.

Bock, Jason B., Richard C. Lin, and Richard H. Scheller. 1996. 'A New Syntaxin Family Member Implicated in Targeting of Intracellular Transport Vesicles', *Journal of Biological Chemistry*, 271: 17961-65.

Boden, Guenther, Isabel G. Ryan, Brenda L. Eisenschmid, John J. Shelmet, and Oliver E. Owen. 1986. 'Treatment of Inoperable Glucagonoma with the Long-Acting Somatostatin Analogue SMS 201–995', *New England Journal of Medicine*, 314: 1686-89.

Borgeat, Pierre, Fernand Labrie, Jacques Drouin, Alain Bélanger, Hans Immer, K. Sestanj, V. Nelson, Manfred Gótz, Andrew V. Schally, David H. Coy, and Esther J. Coy. 1974. 'Inhibition of adenosine 3',5'-monophosphate accumulation in anterior pituitary gland in vitro by growth hormone-release inhibiting hormone', *Biochemical and Biophysical Research Communications*, 56: 1052-59.

Bos, K., C. Wraight, and K. K. Stanley. 1993. 'TGN38 is maintained in the trans-Golgi network by a tyrosine-containing motif in the cytoplasmic domain', *The EMBO Journal*, 12: 2219-28.

Bourdoncle, Pierre. 2006. 'Colocalization', Accessed July 30, 2015. http://rsb.info.nih.gov/ij/plugins/colocalization.html.

Brazeau, Paul, Wylie Vale, Roger Burgus, Nicholas Ling, Madalyn Butcher, Jean Rivier, and Roger Guillemin. 1973. 'Hypothalamic Polypeptide That Inhibits the Secretion of Immunoreactive Pituitary Growth Hormone', *Science*, 179: 77-79.

Bucci, Cecilia, Robert G. Parton, Ian H. Mather, Henk Stunnenberg, Kai Simons, Bernard Hoflack, and Marino Zerial. 1992. 'The small GTPase rab5 functions as a regulatory factor in the early endocytic pathway', *Cell*, 70: 715-28.

Buckmaster, Paul S., Veronica Otero-Corchón, Marcelo Rubinstein, and Malcolm J. Low. 2002. 'Heightened seizure severity in somatostatin knockout mice', *Epilepsy Research*, 48: 43-56.

Carroll, Kate S., John Hanna, Iris Simon, Jeff Krise, Pierre Barbero, and Suzanne R. Pfeffer. 2001. 'Role of Rab9 GTPase in Facilitating Receptor Recruitment by TIP47', *Science*, 292: 1373-76.

Chen, Annie, Enno K. Göβling, Leora Witkowski, Amar Bhindi, Carola Bauch, Geneviève Roussy, Philippe Sarret, Hans-Jürgen Kreienkamp, and Thomas Stroh. 2012. 'Regional and subcellular distribution of the receptor-targeting protein PIST in the rat central nervous system', *The Journal of Comparative Neurology*, 520: 889-913.

Craft, S., S. Asthana, J. W. Newcomer, and et al. 1999. 'ENhancement of memory in alzheimer disease with insulin and somatostatin, but not glucose', *Archives of General Psychiatry*, 56: 1135-40.

Csaba, Z., and P. Dournaud. 2001. 'Cellular biology of somatostatin receptors', *Neuropeptides*, 35: 1-23.

Csaba, Z., B. Lelouvier, C. Viollet, V. El Ghouzzi, K. Toyama, C. Videau, V. Bernard, and P. Dournaud. 2007. 'Activated somatostatin type 2 receptors traffic in vivo in central neurons from dendrites to the trans Golgi before recycling', *Traffic*, 8: 820-34.

Cuevas-Ramos, D., and M. Fleseriu. 2014. 'Somatostatin receptor ligands and resistance to treatment in pituitary adenomas', *J Mol Endocrinol*, 52: R223-40.

Delprato, Anna, Eric Merithew, and David G. Lambright. 2004. 'Structure, Exchange Determinants, and Family-Wide Rab Specificity of the Tandem Helical Bundle and Vps9 Domains of Rabex-5', *Cell*, 118: 607-17.

Díaz, Elva, and Suzanne R. Pfeffer. 1998. 'TIP47: A Cargo Selection Device for Mannose 6-Phosphate Receptor Trafficking', *Cell*, 93: 433-43.

Dubois, M. P. 1975. 'Immunoreactive somatostatin is present in discrete cells of the endocrine pancreas', *Proceedings of the National Academy of Sciences of the United States of America*, 72: 1340-43.

Dunn, Kenneth W., Malgorzata M. Kamocka, and John H. McDonald. 2011. *A practical guide to evaluating colocalization in biological microscopy*.

Emery, P. T. J., N. B. Higgs, A. C. Warhurst, G. L. Carlson, and G. Warhurst. 2002. 'Anti-secretory properties of non-peptide somatostatin receptor agonists in isolated rat colon: luminal activity and possible interaction with p-glycoprotein', *British Journal of Pharmacology*, 135: 1443-48.

Epelbaum, Jacques. 1986. 'Somatostatin in the central nervous system: Physiology and pathological modifications', *Progress in Neurobiology*, 27: 63-100.

Ezzat, Shereen, Peter J. Snyder, William F. Young, Louis D. Boyajy, Connie Newman, Anne Klibanski, Mark E. Molitch, Aubrey E. Boyd, Leslie Sheeler, David M. Cook, William B. Malarkey, Ivor Jackson, Mary Lee Vance, Michael O. Thorner, Ariel Barkan, Lawrence A. Frohman, and Shlomo Melmed. 1992. 'Octreotide Treatment of AcromegalyA Randomized, Multicenter Study', *Annals of Internal Medicine*, 117: 711-18.

Fasshauer, Dirk. 2003. 'Structural insights into the SNARE mechanism', *Biochimica et Biophysica Acta (BBA) - Molecular Cell Research*, 1641: 87-97.

Finley, J. C. W., J. L. Maderdrut, L. J. Roger, and P. Petrusz. 1981. 'The immunocytochemical localization of somatostatin-containing neurons in the rat central nervous system', *Neuroscience*, 6: 2173-92.

Florio, Tullio. 2008. 'Somatostatin/somatostatin receptor signalling: Phosphotyrosine phosphatases', *Mol Cell Endocrinol*, 286: 40-48.

Gkouvatsos, Konstantinos, George Papanikolaou, and Kostas Pantopoulos. 2012. 'Regulation of iron transport and the role of transferrin', *Biochimica et Biophysica Acta (BBA) - General Subjects*, 1820: 188-202.

Grant, M., and U. Kumar. 2010. 'The role of G-proteins in the dimerisation of human somatostatin receptor types 2 and 5', *Regul Pept*, 159: 3-8.

Grant, Michael, Haydar Alturaihi, Philippe Jaquet, Brian Collier, and Ujendra Kumar. 2008. 'Cell growth inhibition and functioning of human somatostatin receptor type 2 are modulated by receptor heterodimerization', *Mol Endocrinol*, 22: 2278-92.

Gu, F., C. M. Crump, and G. Thomas. 2001. 'Trans-Golgi network sorting', *Cellular and molecular life sciences : CMLS*, 58: 1067-84.

Heaney, Anthony P., and Shlomo Melmed. 2004. 'Molecular targets in pituitary tumours', *Nat Rev Cancer*, 4: 285-95.

Heisler, S., T. D. Reisine, V. Y. Hook, and J. Axelrod. 1982. 'Somatostatin inhibits multireceptor stimulation of cyclic AMP formation and corticotropin secretion in mouse pituitary tumor cells', *Proceedings of the National Academy of Sciences of the United States of America*, 79: 6502-06.

Hofland, Leo J., and Steven W. J. Lamberts. 2003. 'The Pathophysiological Consequences of Somatostatin Receptor Internalization and Resistance', *Endocrine Reviews*, 24: 28-47.

Hong, Wanjin. 2005. 'SNAREs and traffic', *Biochimica et Biophysica Acta (BBA) - Molecular Cell Research*, 1744: 120-44.

Jackson, Catherine L., and James E. Casanova. 2000. 'Turning on ARF: the Sec7 family of guanine-nucleotide-exchange factors', *Trends in Cell Biology*, 10: 60-67.

Jacobs, S., and S. Schulz. 2008. 'Intracellular trafficking of somatostatin receptors', *Mol Cell Endocrinol*, 286: 58-62.

Jahn, Reinhard, and Richard H. Scheller. 2006. 'SNAREs - engines for membrane fusion', *Nat Rev Mol Cell Biol*, 7: 631-43.

Janecka, A., M. Zubrzycka, and T. Janecki. 2001. 'Somatostatin analogs', *The Journal of Peptide Research*, 58: 91-107.

Johansson, O., T. Hökfelt, and R. P. Elde. 1984. 'Immunohistochemical distribution of somatostatin-like immunoreactivity in the central nervous system of the adult rat', *Neuroscience*, 13: 265-IN2.

Jung, Jae-Joon, Shivangi M Inamdar, Ajit Tiwari, and Amit Choudhury. 2012. 'Regulation of intracellular membrane trafficking and cell dynamics by syntaxin-6', *Bioscience Reports*, 32: 383-91.

Kreienkamp, Hans-Jürgen. 2002. 'Organisation of G-protein-coupled receptor signalling complexes by scaffolding proteins', *Current Opinion in Pharmacology*, 2: 581-86.

Lamberts, Steven W.J., Aart-Jan van der Lely, Wouter W. de Herder, and Leo J. Hofland. 1996. 'Octreotide', *New England Journal of Medicine*, 334: 246-54.

Laporte, Stéphane A., Robert H. Oakley, Jie Zhang, Jason A. Holt, Stephen S. G. Ferguson, Mark G. Caron, and Larry S. Barak. 1999. 'The β2-adrenergic receptor / βarrestin complex recruits the clathrin adaptor AP-2 during endocytosis', *Procedures of the National Academy of Science*, 96: 3712-17.

Liu, Q., R. Cescato, D. A. Dewi, J. Rivier, J. C. Reubi, and A. Schonbrunn. 2005. 'Receptor signaling and endocytosis are differentially regulated by somatostatin analogs', *Mol Pharmacol*, 68: 90-101.

Luzio, J. P., B. Brake, G. Banting, K. E. Howell, P. Braghetta, and K. K. Stanley. 1990. 'Identification, sequencing and expression of an integral membrane protein of the trans-Golgi network (TGN38)', *Biochemical Journal*, 270: 97-102.

Mascardo, Renato N., and Peter Sherline. 1982. 'Somatostatin Inhibits Rapid Centralsomal Separation and Cell Proliferation Induced by Epidermal Growth Factor', *Endocrinology*, 111: 1394-96.

McLauchlan, Hilary, Jane Newell, Nick Morrice, Andrew Osborne, Michele West, and Elizabeth Smythe. 1998. 'A novel role for Rab5–GDI in ligand sequestration into clathrin-coated pits', *Current Biology*, 8: 34-45.

Melmed, Shlomo. 2006. 'Acromegaly', *New England Journal of Medicine*, 355: 2558-73.

Mollenhauer, Hilton H., D. James Morré, and Loyd D. Rowe. 1990. 'Alteration of intracellular traffic by monensin; mechanism, specificity and relationship to toxicity', *Biochimica et Biophysica Acta (BBA) - Reviews on Biomembranes*, 1031: 225-46.

Møller, Lars Neisig, Carsten Enggaard Stidsen, Bolette Hartmann, and Jens Juul Holst. 2003. 'Somatostatin receptors', *Biochimica et Biophysica Acta (BBA) - Biomembranes*, 1616: 1-84.

Nebenführ, Andreas, Christophe Ritzenthaler, and D. Robinson Robinson. 2002. 'Brefeldin A: Deciphering an Enigmatic Inhibitor of Secretion', *Plant Physiology*, 130: 1102-08.

Neudauer, Cheryl L., Gérard Joberty, and Ian G. Macara. 2001. 'PIST: A Novel PDZ/Coiled-Coil Domain Binding Partner for the Rho-Family GTPase TC10', *Biochemical and Biophysical Research Communications*, 280: 541-47.

Nielsen, Erik, Fedor Severin, Jonathan M. Backer, Anthony A. Hyman, and Marino Zerial. 1999. 'Rab5 regulates motility of early endosomes on microtubules', *Nat Cell Biol*, 1: 376-82.

Oakley, Robert H., Stéphane A. Laporte, Jason A. Holt, Marc G. Caron, and Larry S. Barak. 2000. 'Differential Affinities of Visual Arrestin, βArrestin1, and βArrestin2 for G Protein-coupled Receptors Delineate Two Major Classes of Receptors', *Journal of Biological Chemistry*, 275: 17201-10.

Pagès, Philippe, Naoual Benali, Nathalie Saint-Laurent, Jean-Pierre Estève, Andrew V. Schally, Jean Tkaczuk, Nicole Vaysse, Christiane Susini, and Louis Buscail. 1999. 'sst2 Somatostatin Receptor Mediates Cell Cycle Arrest and Induction of p27 Kip1 : EVIDENCE FOR THE ROLE OF SHP-1', *Journal of Biological Chemistry*, 274: 15186-93.

Patel, Y. C., M. T. Greenwood, A. Warszynska, R. Panetta, and C. B. Srikant. 1994. 'All Five Cloned Human Somatostatin Receptors (hSSTR1-5) Are Functionally Coupled to Adenylyl Cyclase', *Biochemical and Biophysical Research Communications*, 198: 605-12.

Patel, Yogesh C. 1999. 'Somatostatin and Its Receptor Family', *Frontiers in Neuroendocrinology*, 20: 157-98.

Patel, Yogesh C., M. T. Greenwood, R. Panetta, L. Demchyshyn, H. Niznik, and C. B. Srikant. 1995. 'Mini Review: The Somatostatin Receptor Family', *Life Sciences*, 57: 1249-65.

Pitcher, Julie A., Neil J. Freedman, and Robert J. Lefkowitz. 1998. 'G Protein-Coupled Receptor Kinases', *Annual Review of Biochemistry*, 67: 653-92.

Pradayrol, L., J. A. Chayvialle, M. Carlquist, and V. Mutt. 1978. 'Isolation of a porcine intestinal peptide with C-terminal somatostatin', *Biochemical and Biophysical Research Communications*, 85: 701-08.

Pradayrol, Lucien, Hans Jörnvall, Victor Mutt, and André Ribet. 1980. 'N-Terminally Extended Somatostatin: The Primary Structure of Somatostatin 28', *FEBS Lett*, 109: 55-58.

Reubi, Jean, Beatrice Waser, Jean-Claude Schaer, and JeanA Laissue. 2001. 'Somatostatin receptor sst1–sst5 expression in normal and neoplastic human tissues using receptor autoradiography with subtype-selective ligands', *European Journal of Nuclear Medicine*, 28: 836-46.

Richardson, U. Ingrid, and Agnes Schonbrunn. 1981. 'Inhibition of Adrenocorticotropin Secretion by Somatostatin in Pituitary Cells in Culture', *Endocrinology*, 108: 281-90.

Riederer, M A, T Soldati, A D Shapiro, J Lin, and S R Pfeffer. 1994. 'Lysosome biogenesis requires Rab9 function and receptor recycling from endosomes to the trans-Golgi network', *The Journal of Cell Biology*, 125: 573-82.

Rivier, J., M. Brown, and W. Vale. 1975. 'D-Trp8-somatostatin: An analog of somatostatin more potent than the native molecule', *Biochemical and Biophysical Research Communications*, 65: 746-51.

Robbins, Richard J., Michael L. Brines, Jung H. Kim, Thomas Adrian, Nihal De Lanerolle, Susan Welsh, and Dennis D. Spencer. 1991. 'A selective loss of somatostatin in the hippocampus of patients with temporal lobe epilepsy', *Annals of Neurology*, 29: 325-32.

Rohrer, Susan P., Elizabeth T. Birzin, Ralph T. Mosley, Scott C. Berk, Steven M. Hutchins, Dong-Ming Shen, Yusheng Xiong, Edward C. Hayes, Rupa M. Parmar, Forrest Foor, Sudha W. Mitra, Sylvia J. Degrado, Min Shu, John M. Klopp, Sheng-Jian Cai, Allan Blake, Wanda W. S. Chan, Alex Pasternak, Lihu Yang, Arthur A. Patchett, Roy G. Smith, Kevin T. Chapman, and James M. Schaeffer. 1998. 'Rapid Identification of Subtype-Selective Agonists of the Somatostatin Receptor Through Combinatorial Chemistry', *Science*, 282: 737-40.

Roland, Joseph T., Anne K. Kenworthy, Johan Peranen, Steve Caplan, and James R. Goldenring. 2007. 'Myosin Vb Interacts with Rab8a on a Tubular Network Containing EHD1 and EHD3', *Molecular Biology of the Cell*, 18: 2828-37.

Roquemore, Elizabeth P., and George Banting. 1998. 'Efficient Trafficking of TGN38 from the Endosome to the trans-Golgi Network Requires a Free Hydroxyl Group at Position 331 in the Cytosolic Domain', *Molecular Biology of the Cell*, 9: 2125-44.

Sarret, P., M. J. Esdaile, P. S. McPherson, A. Schonbrunn, H. J. Kreienkamp, and A. Beaudet. 2004. 'Role of amphiphysin II in somatostatin receptor trafficking in neuroendocrine cells', *J Biol Chem*, 279: 8029-37.

Sciaky, Noah, John Presley, Carolyn Smith, Kristien J. M. Zaal, Nelson Cole, Jorge E. Moreira, Mark Terasaki, Eric Siggia, and Jennifer Lippincott-Schwartz. 1997. 'Golgi Tubule Traffic and the Effects of Brefeldin A Visualized in Living Cells', *The Journal of Cell Biology*, 139: 1137-55.

Seachrist, Jennifer L., and Stephen S. G. Ferguson. 2003. 'Regulation of G protein-coupled receptor endocytosis and trafficking by Rab GTPases', *Life Sciences*, 74: 225-35.

Seger, Rony, and Edwin G. Krebs. 1995. 'The MAPK signaling cascade', *The FASEB Journal*, 9: 726-35.

Shapiro, Mark S., and Bertil Hille. 1993. 'Substance P and somatostatin inhibit calcium channels in rat sympathetic neurons via different G protein pathwavs', *Neuron*, 10: 11-20.

Sharif, N., L. Gendron, J. Wowchuk, P. Sarret, J. Mazella, A. Beaudet, and T. Stroh. 2007. 'Coexpression of somatostatin receptor subtype 5 affects internalization and trafficking of somatostatin receptor subtype 2', *Endocrinology*, 148: 2095-105.

Simonsen, Anne, Jean-Michel Gaullier, Antonello D'Arrigo, and Harald Stenmark. 1999. 'The Rab5 Effector EEA1 Interacts Directly with Syntaxin-6', *Journal of Biological Chemistry*, 274: 28857-60.

Stenmark, Harald. 2009. 'Rab GTPases as coordinators of vesicle traffic', *Nat Rev Mol Cell Biol*, 10: 513-25.

Stroh, Thomas, Alexander C. Jackson, Philippe Sarret, Claude Dal Farra, Jean-Pierre Vincent, Hans-Jürgen Kreienkamp, Jean Mazella, and Alain Beaudet. 2000. 'Intracellular Dynamics of sst5 Receptor in Transfected COS-7 Cells: Maintenance of Cell Surface Receptors during Ligand-Induced Endocytosis', *Endocrinology*, 141: 354-65.

Strowski, M. Z., R. M. Parmar, A. D. Blake, and J. M. Schaeffer. 2000. 'Somatostatin Inhibits Insulin and Glucagon Secretion via Two Receptor Subtypes: An in Vitro Study of Pancreatic Islets from Somatostatin Receptor 2 Knockout Mice', *Endocrinology*, 141: 111-17.

Takano, K., J. Yasufuku-Takano, T. Kozasa, S. Nakajima, and Y. Nakajima. 1997. 'Different G proteins mediate somatostatin-induced inward rectifier K+ currents in murine brain and endocrine cells', *The Journal of Physiology*, 502: 559-67.

Tiwari, Ajit, Jae-Joon Jung, Shivangi M. Inamdar, Charles O. Brown, Apollina Goel, and Amit Choudhury. 2011. 'Endothelial Cell Migration on Fibronectin Is Regulated by Syntaxin 6-mediated α5β1 Integrin Recycling', *Journal of Biological Chemistry*, 286: 36749-61.

Trischler, M., W. Stoorvogel, and O. Ullrich. 1999. 'Biochemical analysis of distinct Rab5- and Rab11-positive endosomes along the transferrin pathway', *Journal of Cell Science*, 112: 4773-83.

Tsaneva-Atanasova, Krasimira, Arthur Sherman, Frederick van Goor, and Stanko S. Stojilkovic. 2007. *Mechanism of Spontaneous and Receptor-Controlled Electrical Activity in Pituitary Somatotrophs: Experiments and Theory*.

Tulipano, G., R. Stumm, M. Pfeiffer, H. J. Kreienkamp, V. Hollt, and S. Schulz. 2004. 'Differential beta-arrestin trafficking and endosomal sorting of somatostatin receptor subtypes', *J Biol Chem*, 279: 21374-82.

Ullrich, O, S Reinsch, S Urbé, M Zerial, and R G Parton. 1996. 'Rab11 regulates recycling through the pericentriolar recycling endosome', *The Journal of Cell Biology*, 135: 913-24.

Ullrich, O, H Stenmark, K Alexandrov, L A Huber, K Kaibuchi, T Sasaki, Y Takai, and M Zerial. 1993. 'Rab GDP dissociation inhibitor as a general regulator for the membrane association of rab proteins', *Journal of Biological Chemistry*, 268: 18143-50.

Vale, Wylie, Catherine Rivier, Paul Brazeau, and Roger Guillemin. 1974. 'Effects of Somatostatin on the Secretion of Thyrotropin and Prolactin', *Endocrinology*, 95: 968-77.

Wagner, M., A.K. Rajasekaran, D.K. Hanzel, S. Mayor, and E. Rodriguez-Boulan. 1994. 'Brefeldin A causes structural and functional alterations of the trans-Golgi network of MDCK cells', *Journal of Cell Science*, 107: 933-43.

Wang, Zhiping, Jeffrey G. Edwards, Nathan Riley, D. William Provance Jr, Ryan Karcher, Xiang-dong Li, Ian G. Davison, Mitsuo Ikebe, John A. Mercer, Julie A. Kauer, and Michael D. Ehlers. 2008. 'Myosin Vb Mobilizes Recycling Endosomes and AMPA Receptors for Postsynaptic Plasticity', *Cell*, 135: 535-48.

Wendler, Franz, Lesley Page, Sylvie Urbé, and Sharon A. Tooze. 2001. 'Homotypic Fusion of Immature Secretory Granules During Maturation Requires Syntaxin 6', *Molecular Biology of the Cell*, 12: 1699-709.

Wente, Wolf, Thomas Stroh, Alain Beaudet, Dietmar Richter, and Hans-Jürgen Kreienkamp. 2005. 'Interactions with PDZ Domain Proteins PIST/GOPC and PDZK1 Regulate Intracellular Sorting of the Somatostatin Receptor Subtype 5', *Journal of Biological Chemistry*, 280: 32419-25.

Woodman, Philip G. 2000. 'Biogenesis of the Sorting Endosome: The Role of Rab5', *Traffic*, 1: 695-701.

Zerial, Marino, and Heidi McBride. 2001. 'Rab proteins as membrane organizers', *Nat Rev Mol Cell Biol*, 2: 107-17.